The activation and the spreading of deformation in a fully lamellar Ti-47Al-1Cr-0.2Si Alloy

Jung Bahadur Singh, Guy Molénat, M. Sundararaman, Srikumar Banerjee, Georges Saada, Patrick Veyssière, Alain Couret

The activation and the spreading of deformation in a fully lamellar Ti-47Al-1Cr-0.2Si Alloy

Journal:	*Philosophical Magazine & Philosophical Magazine Letters*
Manuscript ID:	TPHM-05-Nov-0485.R1
Journal Selection:	Philosophical Magazine
Date Submitted by the Author:	20-Jan-2006
Complete List of Authors:	Singh, Jung Bahadur; Bhabha Atomic Research Centre, Materials Science Division Molénat, Guy; CEMES-CNRS, , BP 94347 Sundararaman, M.; Bhabha Atomic Research Centre, Materials Science Division Banerjee, Srikumar; Bhabha Atomic Research Centre, Materials Science Division Saada, Georges; CNRS-ONERA, LEM Veyssière, Patrick; CNRS-ONERA, Laboratoire d Etude des Microstructures; CNRS-ONERA, LEM Couret, Alain; CEMES - CNRS, BP 94347
Keywords:	titanium aluminides, deformation, dislocations, stress analysis, TEM
Keywords (user supplied):	

The activation and the spreading of deformation in a fully lamellar Ti-47Al-1Cr-0.2Si Alloy

J. B. Singh[a], G. Molénat[b], M. Sundararaman[a], S. Banerjee[a], G. Saada[c], P. Veyssière[c] and A. Couret[b*],

[a]*Materials Science Division, Bhabha Atomic Research Centre, Mumbai, India*
[b]*CEMES, CNRS, BP 94347, Toulouse, France*
[c]*LEM, CNRS-ONERA, BP 72, 92322 Châtillon, France*

Abstract

The spreading of deformation in a lamellar Ti-47Al-1Cr-0.2Si alloy deformed under compression is studied at 25°C and 600 °C. This microstructure is largely dominated by twin related variants which are separated by either twin interfaces or thin α_2 slabs.

The alloy deforms at both temperatures by ordinary dislocations and twins. Deformation in a particular γ variant and its adjacent twin-related variant involves the same kind of glide system, either ordinary dislocations or twins. This property is found to be true for all twin related lamellae. The occurrence of this correlated glide is explained by the introduction of the notion of "*pilot*" and "*driven*" orientations. The lamellar orientation in which the operating glide system is activated on the basis of Schmid factor considerations is termed the *pilot* orientation. It imposes its deformation system on to the twin-related lamella, called the *driven* orientation whose deformation may not involve the slip system most favoured by the applied stress.

1 INTRODUCTION

γ-TiAl-based two-phase alloys can be processed to achieve several kinds of microstructures such as fully lamellar, nearly lamellar and duplex structures. The fully lamellar microstructure exhibits improved creep strength and fracture toughness, albeit at the expense of tensile elongation properties [1]. The lamellar structure is formed when the alloy is heat-treated or hot-worked above the α transus [2, 3] followed by cooling and evolves according to the following sequence:

$$\alpha \rightarrow \alpha + \gamma \rightarrow \alpha_2 + \gamma$$

* Author for correspondence. Email: couret@cemes.fr

The microstructure is comprised of a stacking of γ ($L1_0$ structure) and α_2 ($D0_{19}$ structure) lamellae whose interfaces lie along compact planes obeying the following orientation relationships [4]:

$$\{111\}_\gamma // (0001)_{\alpha 2} \text{ and } \quad <1\bar{1}0]_\gamma // <11\bar{2}0>_{\alpha 2}$$

The <uvw] mixed bracket notation is used in order to indicate that all permutations amongst u and v are allowed while the third index is fixed [5]. In the $L1_0$ structure, rows along the <110] directions are made of identical atoms whereas Ti and Al atoms alternate along the <101] directions. As a result, the γ-phase exhibits six different variants differing by the stacking sequence along the normal of the {111} interface (as …ABCABC… or …ACBACB…) and/or by the relative orientations of the <110] monoatomic row in the planes parallel to the interface [6]. This results in the formation of three different types of γ/γ interfaces in addition to the γ/α_2 interface in the lamellar structure. Experimentally, it is observed that the distribution of γ–variants within a grain is not random: true-twin γ/γ interface are favoured over order and pseudo-twin interfaces [7].

Compared to the γ phase, the α_2 phase is more resistant to deformation and it is generally considered that in the two-phase TiAl alloys, plasticity is restricted to the γ phase. We have recently shown that whereas some α_2 lamellae deformed at room temperature exhibit some dislocation activity, most of the transfer of plasticity across α_2 lamellae occurs by elastic shear [8]. This is why this paper addresses the plasticity of the γ phase only. We recall that in the $L1_0$ structure, dislocations with Burgers vectors 1/2<110] (the so-called "ordinary dislocations"), <011] and 1/2<112] superdislocations glide on {111} close-packed planes leaving the long-range order undisturbed as they are all unit translations of the $L1_0$ structure.

In polycrystalline two-phase TiAl alloys, the primary deformation mode is by glide of ordinary dislocations accompanied by true twinning [1,9]. It is recalled that given a {111} plane of the $L1_0$ structure, there is only one Shockley partial, i.e. $1/6<11\bar{2}]$, that generates intrinsic stacking faults without first-neighbours violations. Shear in the opposite direction, $1/6<\bar{1}\bar{1}2]$, the anti-twinning mode, would produce extrinsic stacking faults. On the other hand, 1/6<211] Shockley partials would disturb the long-range order forming "pseudo-twins", which, as per our knowledge, have never been observed in TiAl alloys.

This paper reports on an investigation of the glide systems activated at two temperatures (25°C and 600°C), and of the factors controlling this activation in a polycrystalline lamellar TiAl alloy. The study is based on a local analysis of Schmid factors. Such questions had been

previously addressed in the case of polysynthetically twinned crystals deformed in compression as well as tension [10] and in fatigue [11], both investigations indicate the importance of the continuity of the macroscopic strain at lamellar boundaries. In the latter work, Schmid law violations have been evidenced at mismatched interfaces for the case of samples oriented in the hard mode [6], leading to the conclusion that in determining the activated deformation modes, the continuity of macroscopic strain takes over the continuity of glide planes and over Schmid factors.

2 EXPERIMENTAL PROCEDURE

2.1 Alloy preparation

Arc melted buttons of Ti-47Al-1Cr-0.2Si (expressed in atomic percentage) were kindly provided by DMMP, ONERA, Châtillon, France. The as-received buttons were homogenized at 1400°C for 3 h in a platinum furnace under flowing argon atmosphere, followed by cooling at a rate of about 15°C/min between 1400 and 900°C. The pick-up of the trace oxygen as well as moisture from the flowing gas was prevented by covering the alloy button by a thin molybdenum foil with a tungsten separator and as well as by placing a green pellet of titanium sponge in the furnace immediately before the sample in front of the incoming gas stream. This treatment was found to be sufficient to homogenize the alloy as well as to break the cast structure. The final average grain size was about 3 mm.

2.2 Mechanical tests

Compression samples with square cross-section (about 5x5x10 mm^3) were cut from the homogenized alloy by electric discharge machining (EDM). The samples were compression tested in an Instron testing machine at 25°C and 600°C at a strain rate of 3.33×10^{-4} per second. Deformation was stopped at a strain of about 2%. The 0.2% offset yield stresses for these samples were 335 and 260 MPa, respectively. It is however to be noted that, because the grain size is of the order of the sample dimension, and because various distinct deformation systems can be activated depending on Schmid factors, deformation microstructure may differ from one sample to another tested at the same temperature. The above yield-stress values are therefore subject to a significant scatter but we have checked that the above trend (i.e., the yield stress is the highest at 25°C) is unchanged.

2.3 Transmission Electron Microscopy Investigations

For transmission electron microscopy (TEM) investigations, slices of about 0.3 mm in thickness were cut by EDM at 45° and 90° to the compression face. Different directions were marked on the samples prior to cutting in order to keep track of the compression axis in the TEM foils. The slices were mechanically ground to about 0.1 mm thickness prior to being electrolytically thinned to perforation in a 6% perchloric acid and 94% butanol solution using a Fischione twin-jet electropolisher. The temperature of the electrolyte and the current were maintained at about -40°C and 20 mA, respectively. The thin foils were investigated in a JEOL 2010 transmission electron microscope at CEMES, Toulouse, France.

A number of foils were investigated by TEM. Throughout the paper, the lamellar interfaces are designated as (111). Dislocation Burgers vectors were determined by the standard **g.b** = 0 invisibility criterion. Whenever necessary, the glide plane was identified from the dependence of the apparent width of curved dislocation segments on tilt angle.

The microstructure of the undeformed alloy was characterized based on a statistical analysis of adjacent lamellae in two samples. Table 1 exemplifies this analysis on 72 contiguous lamellae comprising 52 γ and 20 α_2 lamellae whose average widths are 340 nm and 115 nm, respectively. Lamellae of the γ phase with different orientations are designated O1, O2, O3, OT1, OT2 and OT3 such that O1, O2 and O3 are in true-twin orientation with OT1, OT2 and OT3, respectively. As already reported for several lamellar TiAl alloys [12], Table 1 shows that one orientation clearly prevails (here O1) together with its twin (OT1). It is worth mentioning that the designation of the dominant lamellae may differ from one sample to another since that depends on the initial choice, which is arbitrary, made for the reference orientation.

3 RESULTS

3.1 The microstructure of the alloy deformed at 600 °C

The microstructure representative of deformation at 600°C is illustrated in figures 1 to 3. Figure 1 shows a montage including 16 lamellae labelled L1 to L16. Not clearly visible, a very thin α_2 lamella (designated L9) separates the L8 (OT1) and L10 (O1) γ-lamellae. Two types of deformation microstructures can be distinguished. The first type found in lamellae L3, L5, L7 and L10, all with orientation O1, and lamella L8 (orientation OT1), involves only ordinary dislocations all with the same Burgers vector. Although some ordinary dislocations exhibit weak contrast in the upper part of figure 1, the imaging conditions in L7 and L8 are

not good enough here to clearly show the existing microstructural similarity between these and other lamellae. The second type of microstructure, exemplified in L1, L11, L12, L14 and L15 (orientations O2 and OT2) is dominated by twins that coexist with a still significant amount of ordinary dislocations. As expected from previous investigations [8,13], α_2 lamellae exhibit very few dislocations. The above two types of deformation microstructures in γ lamellae are analyzed in the following.

3.1.1 Lamellae with ordinary dislocations

In L3, L5, L7, L8 and L10, the ordinary dislocations exhibit analogous properties and their 1/2[110] Burgers vector does not belong to the interface. They show a preference for the screw orientation and they lie in $(\bar{1}1\bar{1})$ planes inclined to the interface plane (as identified by tilt experiments). In twin-related adjacent lamellae, the Burgers vectors of the gliding ordinary dislocations (projections on plane of observation indicated by an arrow ($\mathbf{b_O}$); for O1 and OT1, see L5 and L8, respectively) are in mirror symmetry with respect to the interface. As already reported in the literature [14,15], these lamellae contain debris such as loops that attest to frequent cross-slip events. Lamellae containing ordinary dislocations with a Burgers vector at an angle to the interface plane represent the most frequent situation, though some cases of a lamella containing ordinary dislocations with Burgers vector parallel to the interface were identified (Fig.2) in another thin foil. The frequent observation of loops anchored at γ/α_2 interfaces (marked "loop" in Fig.1) indicates that emission of ordinary dislocations takes place at γ/α_2 interfaces. This property holds true whether the Burgers vector of ordinary dislocations is parallel or not to the interfaces.

3.1.2 Lamellae containing twins and associated ordinary dislocations

As mentioned earlier, twinning is the predominant mode of deformation in L1, L11, L12, L14 and L15. The twins lie on the $(\bar{1}11)$ planes of the lamellae with O2 and OT2 mirror orientations. The decrease of the twin volume fraction from L15 to L11 indicates that the twin-mediated propagation of strain has proceeded from right to left.

The area boxed in Fig.1 points to some ordinary dislocations that coexist with twins in L12 and originate from the positions where twins are in contact with the L13/L12 interface. The habit plane(s) of some portions of these dislocations ($\mathbf{b}$ = 1/2[110]) were identified by comparison between images all taken under the 220 diffraction vector parallel to the Burgers vector but under different tilt conditions. Fig. 3 shows two images of this tilt series, one with

the sample tilted by –23° (Fig. 3a) and the other tilted by +20° (Fig. 3b). The habit planes of 8 segments, namely **a**, **b**, **c**, **d**, **e**, **f**, **g** and **h**, were analysed from their apparent widths measured perpendicularly to the tilt axis. Segment **c** lie on $(\bar{1}11)$ (nearly edge-on in Fig.3b) while segment **h** is on (001). Segments **d** and **b** are in planes rather close to $(\bar{1}11)$ and (001), respectively while segments **a**, **e**, **f** and **g** lay on planes all located much closer to the (001) plane than to any of the other crystallographic planes considered in the vicinity of (001). Configurations undergoing near-(001) slip are consistent with cube slip interrupted in places by double cross-slip events. The Schmid factors (SFs) for the $1/2[110](\bar{1}11)$, $1/2[110](001)$ and $1/2[110](1\bar{1}1)$ are 0.26, 0.27 and 0.05, respectively, with the former two thus subjected to about the same shear stresses. On account of such a low Schmid factor, 1/2[110](001) is unlikely to have operated under the applied stress only. Rather, it is believed that the twinning partials piled-up at the L13/L14 lamellae interface did contribute significantly to the activation of this glide system. The present analysis is thus in accordance with the observation of Forwood and Gibson [16] explaining how when a twin intersects the interface along the <101] direction, ordinary dislocations are generated at γ/α_2 interfaces and glide on (001) of the lamella containing the incident twin. However, the propagation from right to left of twins suggests that these ordinary dislocations are emitted from twins impinging on the interfaces. The present observations are also consistent with the generation of ordinary dislocations where twins intersect γ/α_2 interfaces as proposed by Forwood et al. [16]. It is indeed likely that twin expansion in general and in L12 in particular, proceeds from a two-stepped mechanism : (i) transmission *per se* of a twin spearhead that occurs locally where the α_2 barrier is the weakest [16,8], (ii) then, propagation of this twin sideways. Since it is unlikely that the exact location where transmission has taken place is contained in the thin foil, one is led to conclude that the above ordinary dislocations have resulted from the impact of the interfaces by laterally expanding twins.

3.1.3 Propagation of shear across interfaces

We analyze twin propagation throughout the L15 to L11 γ–lamellae (Fig. 1). In true-twin related γ–lamellae (such as L14 and L15 in Fig. 1), mechanical twins penetrate the adjacent lamella on a plane in mirror symmetry with respect to the plane of the incident twin [17-19].

Twins nucleating at the L13/L12 γ/α_2-interface together with coexisting ordinary dislocations are arranged as if they had been activated by the internal stresses arising from the

twinning dislocations that had piled-up in the vicinity of the L14/L13 interface (see small white headed arrows in L13 on Fig. 1). The coincidence of positions of twins in L14 and L12 lamellae and a higher density of twin plates in the former indicates that the shear has been transferred from L14 to L12 lamellae through the α_2 (L13) lamella. Since hardly any dislocation contrast is observed in the L13 (α_2) lamella, it supports the hypothesis that the α_2 lamella has transmitted the shear elastically [8].

It can be seen in Fig. 1 that in L10, ordinary dislocations are preferentially localized near areas where twins have impacted the true-twin L12/L11 interface (black short arrows in lamella L11), thus suggesting that this activation of ordinary dislocations in L10 was influenced by the accumulation of stresses due to the pile-up of twinning dislocations at interfaces. The absence of a twinning activity in L11 again suggests that slip activity in L10 is simply elastically-mediated through L11 under the influence of the dislocations (twinning partials and ordinaries) locked at the L12/L11 interface.

3.2 Microstructure of the alloy deformed at 25 °C

Like samples deformed at 600°C, those deformed at room temperature exhibit twins and ordinary dislocations, as previously observed in polysynthetically twinned crystals [20] (Fig. 4). In addition, dislocations with <011] as well as 1/2<112] Burgers vector, which will not be analysed in the present paper, were also observed in places. Again, little evidence of plasticity was detected in α_2 lamellae.

3.2.1 Ordinary Dislocations

γ–lamellae deforming by ordinary dislocations, contain a uniform dislocation population reflecting homogeneous source activation at γ/α_2 interfaces and/or within the lamellae. As in the 600°C-samples, the two orientations of Burgers vectors are observed (i.e. Burgers vectors parallel or inclined to the interface) both giving rise to similar microstructural properties. Figs. 4a and 4b display representative regions where the ordinary dislocations have a Burgers vector parallel and inclined to the interface plane, respectively. They all tend to be elongated in the screw orientation although not as markedly as in the 600°C-samples conforming with previous investigations [21,22]. As the (111) interface plane is close to being edge-on in Fig. 4a, the pronounced apparent curvature indicates that part of the movement took place out of this plane, presumably in $(11\bar{1})$. The density of loops and debris is less than that observed after deformation at 600°C.

3.2.2 *Twinning*

Fig. 4c shows an area containing several O1 and OT1 lamellae containing a fairly homogeneous distribution of twins (the twins lying in L9 (OT1) are hardly visible because of poor contrast conditions). As in samples deformed at 600°C, twins in adjacent true-twin-related lamellae are in mirror symmetry with respect to the interface plane.

3.2.3 *Crossing of twin interfaces by ordinary dislocations*

Fig. 5 shows a pile-up of dislocations straddling a twin interface. The two twin-related lamellae L1 and L2 are separated by an interface inclined at about 10° to the foil normal. The pair of parallel dashed lines embodies the (111) L1/L2 interface considering that the short vertical segments are lying in the interface as explained below (see for instance the dislocation marked a). The 1/2[$\bar{1}$10] Burgers vector of the dislocations is almost parallel (4°) to the thin foil. The curvature of the dislocations indicates that they were moving from the left part to the right part of the observed area. The straight line joining the upper extremities of dislocations in L1 shows that they are piled in the $(11\bar{1})^{L1}$ plane with a marked coplanarity. In lamella L2, the lower extremities of the dislocations situated between (C) and (D) attest to glide having occurred in the $(11\bar{1})^{L2}$ plane. Schmid factors for the 1/2[$\bar{1}$10] dislocations are 0.34, 0.22 and 0.44 in (111), $(11\bar{1})^{L1}$ and $(11\bar{1})^{L2}$ planes, respectively.

The strong edge character of the dislocations of the pile-up (Fig. 5b) is a result of the thin foil surface almost parallel to the Burgers vector, which absorbs the screw portion. It should be underlined that several apparent differences in the microstructural features observed in L1 and L2 (such as the number of debris, the dislocation pinning at the neighbouring interfaces and the proportion of screw segments), originate from the fortuitous asymmetrical orientation of the thin foil with respect to the $(11\bar{1})^{L1}$ and $(11\bar{1})^{L2}$ planes (Fig. 5b). This causes certain limitations in interpreting the configuration such as in which lamella the dislocations were initially moving.

The dislocations located further on the right after mark C appear to straddle L1 and L2. Such a configuration is the result of easy cross-slip of the screw segments at the interface in agreement with similar events previously evidenced by *in situ* straining experiments [19]. Some straddling dislocations exhibit angular points or rectilinear short segments that belong to the interface (see for instance dislocations *a* or *f*). This attests to some glide having occurred in the interface plane before the transfer of these screw segments in the next lamella.

As these segments are lying in the interface, they behave as dragged portions hampering the motion of those located in the lamellae, as is illustrated by the bending of the L2 segment of dislocation *a* and of the L1 segment of dislocation *f*.

4 DISCUSSION

We have confirmed that in Ti-47Al-1Cr-0.2Si alloys compressed at 25°C and 600°C, γ lamellae are predominantly deformed either by ordinary dislocations or by twins. Ordinary dislocations are generated in the lamellae by crossing of dislocations from adjacent lamellae or as a by-product of the interaction of twins with interfaces. Emission of by-product ordinary dislocations allows for the relaxation of internal stresses, probably hampering crack formation. The process is temperature independent.

The present section is devoted to investigating the parameters pivotal to the activation of the predominant deformation mode in a given γ–lamella (§ 4.1) and to quantitatively discuss stress distribution (§ 4.2) in the specific geometry imposed in lamellar TiAl.

4.1 Factors governing slip mode activation in the driven lamellae

On the basis of Tables 2 and 3 for 600°C and room temperature samples, respectively, we analyse the role of (i) the applied stress, (ii) lamella width, and (iii) lamella environment. A number of lamellae (column 2) taken from different samples (column 1) have been analysed for the two temperatures investigated. When the lamellae referred to are taken from images presented in this paper, their labels in the corresponding figures are mentioned in column 3. Column 4 gives the orientation of the lamella analysed with its width expressed in μm in parenthesis. Columns 5 and 6 give the same information for the two adjacent lamellae, on the left-hand side (LHS) and right-hand side (RHS) respectively. Columns 7 and 8 provide the active Schmid factor (SF) for the predominant deformation mode: active SF for ordinary (ASFO) dislocations and active SF for twinning (ASFT). Columns 9 and 10 indicate the highest Schmid factor within each lamella for ordinary dislocations (HSFO) and for twinning (HSFT). In parenthesis in columns 7 and 9 is indicated the angle between the Burgers vector of the corresponding ordinary dislocations and the interface plane (0° or 60°). Finally, column 11 indicates whether the Schmid law applies within each lamella for the active deformation mode. The answer is 'Yes' in lamellae with ordinary dislocations when the ASFO is equal to the HSFO and 'No' otherwise. In order to account for experimental

uncertainties, the answer is also "Yes" when the ASFO is lower than but very close to ($\delta SF \leq -0.05$) the HSFO. The same rule is applied to twinned lamellae.

From these two tables, it appears that the lamellae with a given orientation all deform in the same way by making use of a unique slip system, i.e. only one type of ordinary dislocations or twins. Specimen 25-3 (Table 3) provides a good illustration of this property for ordinary dislocations since all 8 lamellae in the O1 orientation have deformed by the same slip system (with SF = 0.43) whereas an equivalent system of ordinary dislocations (SF = 0.45) was available. In all the investigated specimens, this property is valid *regardless of lamellar thickness*, thus ruling out the lamella width as pertinent parameters in controlling the slip system activation.

Tables 2 and 3 also illustrate that two twin-related lamellae (i.e. O_i and OT_i) exhibit the same predominant deformation mode *whether they are adjacent or separated by an* α_2 *lamella*. That is the case for ordinary dislocations in lamellae 2 to 6, 22 to 24, 26 to 28 in Table 2 and 2 to 4, 5 to 19 (except 10-OT2) in Table 3 and for twins in lamellae 7 to 12 and 14 to 21 in Table 2; 21-22, 26 to 29 in Table 3. Figure 1 provides a fair illustration of these properties.

The following sections are aimed at explaining why twin-related lamellae deform by the same predominant mode.

4.1.1 Ordinary dislocations

Tables 2 and 3 show that out of the two possible orientations of 1/2<110] Burgers vectors (parallel or inclined to the interface plane), one only operates in twin-related adjacent variants. For a Burgers vector parallel to the interface, this property is illustrated by lamellae 26 to 28 of sample 600-3 (table 2), lamellae 1 to 4 of sample 25-1 (table 3) and lamellae 5 to 18 (except 10-OT2) of sample 25-3 (table 3). For a Burgers vector at 60° to the interface, this is seen in the case of lamellae 2 to 6 of sample 600-1 (table 2) and lamellae 22 to 24 of sample 600-2 (table 2). It is worth noting that when in a variant O_i (i = 1 to 3) the Schmid law applies (i.e., $ASFO^{Oi} = HSFO^{Oi}$), then in the conjugate OT_i variant it may (samples 600-3 and 25-1: $ASFO^{OTi} = HSFO^{OTi}$) or not (samples 600-1, 600-2 and 25-3: $ASFO^{OTi} < HSFO^{OTi}$) apply.

A scenario based on the notion of "*pilot*" and "*driven*" orientations explains how a given glide system of ordinary dislocations becomes the only operative system within O_i/OT_i twin-related variants. In this scenario, the O_i orientation that is capable of imposing the operation of given ordinary system in the OT_i orientation is referred to as the *pilot* orientation while the

OT_i orientation itself is called the *driven* orientation. Sources of ordinary dislocations are activated within the lamellae with an O_i orientation, in consistency with the Schmid law ($ASFO^{pilot} = HSFO^{pilot}$ and $ASFO^{pilot} \geq HSFO^{driven}$ of the OT_i conjugate orientation). In other words, the pilot orientation imposes the slip system operating in the twin related conjugate variants, irrespective of the Schmid factor of the latter. The operating Burgers vector may either be inclined to the interface plane (Fig.1 and Fig.4b) or parallel to it (Fig.2 and Fig.4a). Fig. 1 shows this scenario taking place between orientation O1 (lamellae L3, L5, L7, L10) and orientation OT1 (lamella L8) acting as the pilot orientation (ASFO = 0.49) and the driven orientation (ASFO = 0.28 when HSFO = 0.39 is available), respectively. One extreme case is provided by sample 600-2 where the OT2 pilot orientation (lamella 23) imposes a glide system in the O2 driven orientation (lamella 22) with a very unfavourable resolved shear stress (ASFO = 0.04 when HSFO = 0.31 is available). The property that the Schmid factor is instrumental in determining which orientation can act as pilot orientation is found to be independent of the volume fraction of the different variants. This, however, cannot be concluded for certain since slip transfer may not have been initiated in the region observed by TEM but elsewhere the relative abundance of the twin-oriented lamellae is reversed (Pilot > Driven).

Situations of a violation of the Schmid law similar to that exhibited by lamella L7 in sample 25-3 can be encountered too (Fig. 4a). In such a case of not twin related interfaces, Nakano and co-workers [11] have evidenced a similar violation of the Schmid law. They have concluded that the predominant factor in selecting the operative systems is the continuity of macroscopic strains, which imposes that the resultant Burgers vector of the emitted dislocations be parallel and equal in magnitude to that of the incident dislocations (see, however, § 4.3).

Ordinary dislocations having a Burgers vector parallel to the interface cross through interfaces by a simple cross-slip process as illustrated in Fig. 5. Hence no problem is expected for such a transmission from the pilot to the driven orientation. The transmission of an ordinary dislocation whose Burgers vector is at 60° from the interface (e.g. lamellae 2 to 6 in sample 600-1 and 22 to 24 in sample 600-2) is, however, not as easy as reported by Zghal and co workers [19]. They actually reported *in situ* observations of such dislocations impacting an interface between twin-related variants. No transfer at all occurred in this case. In the vicinity of the interface and within the OT_i lamella, these authors nevertheless observed one case of the operation of a source of ordinary dislocations with a Burgers vector lying at 60° from the interface. The observation was interpreted as resulting from the built up of

internal stresses by accumulation of incident dislocations, which is fully supported by the present post-mortem observations.

4.1.2 Twinning mode

Similar situations of a *pilot/driven* pair have been encountered for twinning. This is exemplified by sample 25-5 (Table 3) where orientation OT1 is pilot since $ASFT^{pilot} = HSFT^{pilot}$ whereas O1 is the driven variant ($ASFT^{driven} < HSFT^{driven}$). At least in the area shown in Fig. 4c, it is worth noting that the volume fraction occupied by the pilot orientation is lower than that covered by the driven orientation. Samples 600-1 (lamellae numbers 7-12) and 600-2 (lamellae numbers 14 to 21) are representative of another situation in which the *pilot/driven* concept applies in a slightly different manner. In these last two cases and for the twin-related orientations the ASFT is always that of highest Schmid factor for twinning (HSFT). The Schmid law for twinning is therefore never violated. However, as exemplified by sample 600-1, in the OT2 orientation, the Schmid factor available for ordinary dislocations (HSFO = 0.46) is clearly higher than that for the active twin dislocations (ASFT = 0.18).

Twins thus appear to be preferentially generated in lamellae with the O_i pilot orientation and then expand in the OT_i oriented lamellae by emission from the O_i/OT_i interface of twins in the {111} mirror planes of the O_i twin plane as already observed in several studies [17,18,19]. Fig. 1 also illustrates the situation for twinning with the O2 orientation (lamellae L12 and L15) and OT2 orientation (lamellae L11 and L14) acting as the pilot and the driven orientations, respectively.

4.1.3 A global description of deformation in the lamellar structure

The spreading of strain in the lamellar microstructure requires the crossing of coherent (twin) and mismatched (ordered domains or pseudo-twin) interfaces as well as the propagation of deformation through α_2 slabs. As far as the α_2 lamellae are concerned, it has been recently proposed that strain transfer occurs mainly through the effect of elastic strain field, which activate sources in neighbouring lamellae [8]. In the case of mismatched interfaces Schmid law is often violated. In those cases geometrical factors such as the conservation of the Burgers vectors and the continuity of glide/twin planes are likely to be more critical [10,19,23] in addition to internal stress concentrations due to dislocation pile-ups.

At twin-related interfaces, deformation is transferred through the activation of a conjugate deformation system, with the slip systems of the operating dislocations in mirror symmetry. In fact, the factor predominant in deformation transfer at coherent twin interfaces appears to be the continuity of the glide/twin planes. On the other hand, except for the easy case of ordinary dislocations with Burgers vectors parallel to the interface plane for which crossing occurs by a simple cross-slip, the sum of the Burgers vectors of incident dislocations is not equal to that of the emitted dislocations. In other words, the condition of strain continuity proposed by [10,11] is not obeyed locally at twin interfaces and this suggests an additional effect of internal stresses.

One should keep in mind that the distribution of lamellae is not random. It is actually generated as a result of several transformations that are activated at different temperatures during heat treatment [24]. The high temperature transformation produces wide γ lamellae with a unique orientation. Transformations operating at lower temperatures, above and below the eutecticoid temperature, generate thin lamellae which are twin-related to the existing wide lamellae. In polycrystalline TiAl alloys, this results in a lamellar microstructure dominated by two twin-related orientation variants [7,12]. Clearly, it is this prevalence of adjacent-twin related lamellae in the microstructure that confers the analysis of strain transfer between pilot-driven, adjacent twin-related orientations its full importance.

In summary, deformation is activated in the pilot lamellae in which the activation of either ordinary dislocations or of twins is encouraged by adequate Schmid factors and resolved shear stresses, and these dislocations subsequently invade the driven orientation OT_i, in the twin-related variant.

4.2 Stress transfer

This section summarizes the main results of a theoretical analysis of the conditions under which dislocations can be expelled from the interface into the twin-oriented driven lamella, assuming that at the origin of slip transmission is a finite ensemble of equidistant pilot dislocations blocked at the interface. The account made here is essentially concerned with ordinary dislocations with a Burgers vector inclined to the interface in which case slip transmission can be accompanied by a violation of the Schmid law. Some results concerning twinning dislocations will be briefly summarized too. A full account of this model will be the object of a forthcoming paper.

4.2.1 Slip transfer involving inclined ordinary dislocations

The situation observed experimentally is represented by ordinary dislocations with Burgers vectors **DC** and **D'C** gliding on ADC and AD'C mirror planes on the pilot and the driven lamellae, respectively (Fig. 6(a); ABC is the interface plane). On the one hand, an infinite wall of equidistant dislocations whose Burgers vector **DC** is inclined to the interface would generate a long-range stress field in the twin-oriented lamella. Created at **DC** dislocations of the wall, **D'C** dislocations would leave interfacial edge dislocations with Burgers vector **DD'** (i.e. **DD'** = **DC** - **D'C**) engendering a low angle tilt boundary. **D'C** dislocations can thus be thought of as being repelled by the boundary generating in the driven lamella a deformation compatible with that of the pilot and relaxing the internal long-range stresses. A similar reasoning applies, of course, to **CD'** dislocations gliding towards the interface. On the other hand, the interaction between a single pilot **DC** dislocation and a **D'C** dislocation is attractive hindering emission in the latter lamella. Emission would be similarly impeded in case of a pile-up of pilot dislocations. The properties of a finite array of interfacial pilot dislocations are somewhat intermediate between those of a single dislocation and of an infinite array. One indeed expects that, when the driven dislocations are close to the finite array, the force that the latter exerts on driven dislocations is repulsive, akin to that of an infinite array, whereas it is attractive, akin to that of a single dislocation at large distances from the array.

Consider a finite array of height h of interfacial, equidistant **DC** dislocations. The force d**F*** it exerts on a driven dislocation can be calculated considering the array as an homogenous distribution of infinitesimal dislocations with Burgers vector

$$d\mathbf{b} = g\,\mathbf{b}\,dX \tag{1a}$$

where $g = l^{-1}$ is the reciprocal of the dislocation repeat distance. Integrated over the entire array, the projection df* of d**F*** in the glide direction, assumes the following form

$$f^*(y,q) = \mu g b^2 \varphi(y,q) \tag{2a}$$

where the distances y and q in the driven slip plane and in the interface, respectively are given in units of h. At large distances from the interface the force becomes

$$f^*(y,0) \approx \mu g b^2 \frac{\alpha}{y} \tag{2b}$$

where α is a factor that depends on the geometry of the interaction under consideration and on the Poisson's ratio ($\nu = 1/3$). Given b, g and y, the modulus of α represents the strength of the interaction between the pilot and driven dislocations, which is itself at the origin of slip transmission. The coefficient α is negative ($\alpha = -0.1$). In the case of a single pilot dislocation, the interaction far from the array force is written

$$f = \frac{\alpha\,\mu b^2}{hy} \tag{3}$$

Expression (2b) that can be rewritten as

$$f^*(y,0) = ghf \tag{4}$$

states that at large distances from the array the stress exerted on the driven dislocation is that of a dislocation with Burgers vector *nb*, as is expected. The force *f** (expression (2a)) is plotted in Figure 7(a) versus *y* for various values of *q*. It is seen that, the force is a maximum near the interface ($y \approx 0$). The stress, which is actually large enough to nucleate plastic strain, does not vary significantly within a band of thickness 0.8 *h*. The repulsive effect is the most pronounced in the upper part of the driven lamella. The inset in Figure 7(a) illustrates how the force *f** exerted by the array changes its sign at a certain distance from the interface. It shows in addition that the agreement between *f** and *f* is good at long distances from the interface.

4.2.2 Twinning

The above equations (3) and (4) remain valid and the same reasoning applies in the case of homogeneous twinning regarded as resulting from Shockley dislocations $\boldsymbol{\beta}\mathbf{A}$ and $\boldsymbol{\beta}'\mathbf{A}$ gliding in the pilot and in the driven lamellae, respectively. Here, gb_t is a fixed quantity amounting to 2/3, and the force does not change sign. Remarkably, the coefficient $\alpha\,(=0.22)$ is positive and twice as large as in the above case of slip transmission by perfect dislocations. Figure 7(b) shows that the force is almost uniform across the band section, and that its repulsive effects are manifested at distances comparatively larger than those calculated for a band of perfect dislocations of equal thickness (Figure 7(a)).

In summary, these calculations show that whereas neither a single dislocation nor an infinite dislocation array can generate a stress field adequate to ordinary dislocation emission, a band of finite height can provide the required stress field hence giving rise to a Schmid law violation (e.g. sample 600-1 sample, Figure 1 and Table 2). Beside, the stress field produced by a twin is shown to be favorable to twin emission in a mirror plane (e.g. sample 600-1 and 25-5 samples in Figures 1 and 4c, respectively).

5 CONCLUSIONS

The main results of the present investigation of the deformation systems activated during deformation at 25° and 600°C in a fully lamellar TiAl alloys can be summarized as follows:

- Strain is mainly accommodated by twins and ordinary dislocations.
- In a given lamella, the deformation microstructure is mostly dominated by one system. Secondary systems are seldom activated as the result of interaction between twins and interfaces.
- In a given grain, the members of a given variant family all deform by means of the same slip system regardless of their neighbouring lamellae and of the lamella thickness.
- Deformation is first initiated in a lamellae orientation, termed as the *pilot*, on the basis of Schmid factor considerations. That is true for lamellae deforming by ordinary dislocations as well for lamellae deforming by twinning.
- The deformation mode in adjacent, twin-related variants, the *driven* orientation, is dictated by that of the *pilot* orientation. When deformation occurs by ordinary dislocations, the system activated in the driven orientation is symmetrical to that activated in the pilot orientation. In the case of twinning, twins are emitted in plane in mirror symmetry to the plane of incident twins.
- The continuity of glide/twin planes determines the activated systems in the driven orientation.
- Slip transfer across twin-oriented lamellae necessitates that the interfaces be impacted by slip bands with a finite thickness.

The importance of the pilot/driven mechanism stems from the fact that the lamellar microstructure is largely dominated by two twin-related orientations.

Acknowledgements

The authors acknowledge the Indo-French Centre for the Promotion of Advanced Research, New Delhi for sponsoring this project (No. 2308-3) and for funding the visit of one of the authors (J.B.S.) to Toulouse, France. The authors wish to thank Drs Shigehisa Naka and Marc Thomas of DMMP/ONERA for kindly provide the material and Dr. Rajeev Kapoor of Materials Science Division, B.A.R.C., for his help to carry out deformation experiments.

REFERENCES

[1] APPEL, F., and WAGNER, R., 1998, *Mater. Sci. Eng.,* **R22**, 187.

[2] WILLEY, L.A., and MARGOLIN, H., 1973, *Metals Handbook*, ASM, Metal Park, OH, 8th Edition, vol. 8, p.264.

[3] KIM, Y.-W., 1991, *Microstructure/Property Relationships in Titanium Aluminides and Alloys*, edited by Y.-W. Kim and R.R. Boyer (TMS Warrendale, PA), p. 91.

[4] BLACKBURN, M. J., 1970, *The Science, Technology and Applications of Titanium,* edited by R. Jaffe and N. Promisel (Oxford: Pergamon), p. 633.

[5] HUG, G., LOISEAU, A., and VEYSSIÈRE, P., 1988, *Phil. Mag. A*, **57**, 499.

[6] FUJIWARA, T, NAKAMURA, A., HOSOMI M., NISHITANI, S.R., SHIRAI, Y., YAMAGUCHI Phil. Mag A 1990;61(4):591.

[7] ZGHAL, S., NAKA, S., and COURET, A., 1997, *Acta metall. mater*., 45, 3005.

[8] SINGH, J.B., MOLENAT, G., SUNDARARAMAN, M., BANERJEE, S., SAADA, G., VEYSSIÈRE, P., COURET, A., Submitted to Phil. Mag. letters.

[9] FARENC, S., COUJOU, A., and COURET, A., 1993, *Phil. Mag. A*, 67, 127

[10] KISHIDA, K., INUI, H., and YAMAGUCHI, M., 1998, *Phil. Mag.* A, **78**, 1.

[11] NAKANO T, BIERMANN H, RIEMER M, MUGHRABI H, NAKAI Y, UMAKOSHI Y. Phil. Mag A 2001;81(6):1447

[12] ZGHAL, S., THOMAS, M., NAKA, S., and COURET, A., 2001c, *Phil. Mag.* Letters, 81, 537.

[13] APPEL F, BEAVEN PA,WAGNER R., Acta metal. mater. 1993;41:1721

[14] VIGUIER, B., HEMKER, K.J., BONNEVILLE, J., LOUCHET, F., and MARTIN, J.L., 1995, *Phil. Mag. A.,* **71**, 1295.

[15] SRIRAM, S., DIMIDUK, D.N., HAZZELDINE, P.M., and VASUDEVAN, V.K., 1997, *Phil. Mag. A.,* **76**, 965.

[16] FORWOOD, C.T., and GIBSON, M.A., 2000, *Phil. Mag. A*, 80, 2785

[17] WIEZOREK, J.M.K., ZHANG, X.D., MILLS, M.J., and FRASER, H.L., 1998, *Phil. Mag. A*, **78**, 217.

[18] GIBSON, M.A., and FORWOOD, C.T.,2000, *Phil. Mag. A*, 80, 2747

[19] ZGHAL, S., and COURET, A., 2001, *Phil. Mag.* A, 81,365.

[20] INUI, H., NAKAMURA, A., OH, M. H., and YAMAGUCHI, M., 1992, *Phil. Mag.* A, **66**, 557.

[21] GRÉGORI, F., 1999, PhD Thesis, University of Paris VI, France

[22] GRÉGORI, F. and P. VEYSSIÈRE, *Gamma Titanium Aluminides*, Y.-W. Kim, D.M. Dimiduk, and M.H. Loretto, Editors. 1999, Minerals, Metals & Materials Society: Warrendale. p. 75-82.

[23] ZGHAL, S., COUJOU, A., and COURET, A., 2001, *Phil. Mag.* A, 81, 345.

[24] ZGHAL, S., THOMAS, M., NAKA, S., FINEL, A., COURET, A., Acta metal. mater. 2005;53:2653.

Figure captions

Fig.1. A montage of bright-field (BF) images taken from the 600-1 sample (L1, L3, L5, L7, L8, L10, L11, L12, L14 and L15 are γ lamellae and L2, L4, L6, L9, L13 and L16 are α_2 lamellae). The projected Burgers vectors of ordinary dislocations within O1 and OT1 orientation are shown by arrow as $\boldsymbol{b_o}$ in L5 and L8. A detailed view of the boxed region is given in Fig. 3. The microstructural similarity between L7 and L8 on the one hand and L3, L5, L10 on the other is visible in the upper part on the figure.

Fig.2. A weak-beam micrograph of ordinary dislocations in a γ–lamellae (sample 600-3). The Burgers vector is parallel to the interface plane.

Fig.3. Weak-beam identification of planes containing dislocations of the boxed area of Fig. 1 (L12). Examples at tilt angles θ = -23° and θ = 20°). **g** = 220. The habit planes of segments **a** to **h** have been identified (see text for details).

Fig.4. Samples deformed at room temperature. (a) A montage of images from the 25-3 sample showing ordinary screw dislocations with Burgers vector parallel to the interface plane. (b) BF image of a γ–lamella containing ordinary dislocations whose Burgers vector is inclined to the interface plane (sample 25-4). (c) Deformation by twinning (25-5 sample).

Fig.5. (a) DF image showing ordinary dislocations straddling a twin interface. (b) 3D schematic drawing based on TEM analysis.

Fig.6. The crystallography of slip transmission used in the calculations. (a) The two twin-related Thompson tetrahedral. ADC and AD'C are the pilot and driven slip planes, and ABC is the twin interface. (b) Pilot dislocations have accumulated at the interface forming an array of equidistant **DC** dislocations. (c) A **D'C** dislocation escapes from an infinite interface leaving an edge **DD'** dislocation with a Burgers vector normal to the interface.

Fig.7. Plot of the force f^* versus y, the distance of the driven dislocations from the interface in the slip direction (in units of h) for various values of q (see Figure 5b)). (a) The transmission of perfect dislocations. From bottom to top, the arrow intersects the curves corresponding to q = -0.4, -.03, -0.2, (-0.1 and 0), 0.1, 0.2, 0.3 0.4. (b) The transmission of partial dislocations (twinning). From bottom to top, the arrow intersects the curves corresponding to y = -0.4, -.03, -0.2, (-0.1 and 0), 0.1, 0.2, 0.3 0.4. The inset in (b) is similar to that of (a). The insets compare, as a function of y, the force exerted onto a driven dislocation by an array (thickness h), force f^*, and by a single pilot dislocation, force f.

Table caption

Table 1. Quantitative description of the two-phase microstructure investigated..

Table 2. Summary of the general features and of the deformation modes of the γ lamellae in samples compressed at 600° C.

Table 3. Summary of the general features and of the deformation modes of the γ lamellae in samples compressed at 25° C.

Table 1.

Volume Fractions (%)						
α_2	**γ Matrix**			**γ Twins**		
0.12	0.76			0.12		
	O1	**O2**	**O3**	**OT1**	**OT2**	**OT3**
	0.82	0.07	0.11	0.69	0.30	0.01
Distribution of different γ/α_2 and γ/γ interfaces (%)						
γ/α_2 interfaces	**γ/γ interfaces**					
55	45					
	Ordered domain		**Twin**		**Pseudo-twin**	
	40		40		20	

6 Table 2

Sample id	Lamella No.	Lamellae		OR of Bounding Lamellae		Schmid factors for the activated systems		Highest Schmid factors available		Schmid Law
		id	OR	L.H.S.	R.H.S.	ASFO	ASFT	HSFO	HSFT	
600-1	1	L1	O2 (0.36)	α2 (-)	α2 (0.08)	-	0.38	0.30 (0)	0.39	Yes
(Fig; 1)	2	L3	O1 (0.64)	α2 (0.08)	α2 (0.18)	0.49 (60)	-	0.49 (60)	0.19	Yes
	3	L5	O1 (0.66)	α2 (0.18)	α2 (0.07)	0.49 (60)	-	0.49 (60)	0.19	Yes
	4	L7	O1 (0.23)	α2 (0.07)	OT1 (0.37)	0.49 (60)	-	0.49 (60)	0.19	Yes
	5	L8	OT1 (0.36)	O1 (0.23)	α2 (0.00)	0.28 (60)	-	0.39 (0)	0.31	No
	6	L10	O1 (0.70)	α2 (0.00)	OT2 (0.22)	0.49 (60)	-	0.49 (60)	0.19	Yes
	7	L11	OT2 (0.22)	O1 (0.70)	O2 (1.00)	-	0.18	0.46 (60)	0.18	Yes
	8	L12	O2 (1.00)	OT2 (0.22)	α2 (0.22)	-	0.38	0.30 (0)	0.39	Yes
	9	L14	OT2 (0.08)	α2 (0.22)	O2 (0.36)	-	0.18	0.46 (60)	0.18	Yes
	10	L15	O2 (0.36)	OT2 (0.08)	α2 (0.08)	-	0.38	0.30 (0)	0.39	Yes
	11	-	OT2 (0.17)	OT1 (0.12)	O2 (0.60)	-	0.18	0.46 (60)	0.18	Yes
	12	-	O2 (0.60)	OT2 (0.17)	O1 (0.27)	-	0.38	0.30 (0)	0.39	Yes
	13	-	O1 (0.27)	O2 (0.60)	OT1 (0.13)	0.49 (60)	-	0.49 (60)	0.19	Yes
600-2	14	-	O1 (0.11)	α2 (0.06)	OT1 (0.05)	-	0.40	0.33 (0)	0.40	Yes
	15	-	OT1 (0.05)	O1 (0.11)	O1 (0.04)	-	0.34	0.38 (0)	0.34	Yes
	16	-	O1 (0.04)	OT1 (0.05)	α2 (0.00)	-	0.40	0.33 (0)	0.40	Yes
	17	-	O1(0.83)	α2 (0.00)	α2 (0.52)	-	0.40	0.33 (0)	0.40	Yes
	18	-	OT1 (0.03)	α2 (0.52)	O1 (0.02)	-	0.34	0.38 (0)	0.34	Yes
	19	-	O1 (0.02)	OT1 (0.03)	OT1 (0.06)	-	0.40	0.33 (0)	0.40	Yes
	20	-	OT1 (0.06)	O1 (0.02)	O1 (0.00)	-	0.34	0.38 (0)	0.34	Yes
	21	-	OT1 (0.16)	O1 (0.00)	O1 (0.00)	-	0.34	0.38 (0)	0.34	Yes
	22	-	O2 (0.25)	α2 (0.08)	OT2 (0.10)	0.04 (60)	-	0.31 (0)	0.25	No
	23	-	OT2 (0.10)	O2 (0.25)	α2 (0.06)	0.48 (60)	-	0.48 (60)	0.48	Yes
	24	-	OT2 (0.58)	α2 (0.06)	α2 (0.00)	0.48 (60)	-	0.48 (60)	0.48	Yes
600-3	25		O1 (0.67)	O2 (0.15)	α2 (0.03)	0.39 (0)	-	0.39 (0)	0.41	Yes
(Fig.2)	26	-	O3 (0.51)	O1 (0.57)	O6 (0.03)	0.44 (0)	-	0.49 (60)	0.32	Yes
	27	-	OT3 (0.03)	O3 (0.51)	O3 (0.31)	0.29 (0)	-	0.29 (0)	0.34	Yes
	28	-	O3 (0.31)	OT3 (0.03)	α2 (0.02)	0.44 (0)	-	0.49 (60)	0.32	Yes

Table 3

Sample id	Lamella No.	Lamellae		OR of Bounding Lamellae		Schmid factors for the activated systems		Highest Schmid factors available		Schmid Law
		id	OR	L.H.S.	R.H.S.	ASFO	ASFT	HSFO	HSFT	
25-1	1	-	O1 (0.70)	OT2 (0.38)	α2 (0.42)	0.49 (0)	-	0.49 (0)	0.21	Yes
	2	-	O1 (1.17)	α2 (0.42)	OT1 (0.11)	0.49 (0)	-	0.49 (0)	0.21	Yes
	3	-	OT1 (0.11)	O1 (1.17)	O1 (0.88)	0.44 (0)		0.44 (0)	0.21	Yes
	4	-	O1 (0.88)	OT2 (0.38)	α2 (0.42)	0.49 (0)	-	0.49 (0)	0.21	Yes
25-3	5	-	OT1 (0.12)	α2 (0.25)	O1 (0.60)	0.22 (0)	-	0.33 (0)	0.32	No
(Fig.4a)	6	L1	O1 (0.60)	OT1 (0.12)	α2 (0.05)	0.43 (0)	-	0.45 (60)	0.32	Yes
	7	L3	O1 (0.85)	α2 (0.05)	O4 (0.22)	0.43 (0)	-	0.45 (60)	0.32	Yes
	8	L4	OT1 (0.22)	O1 (0.85)	O1 (1.12)	0.22 (0)	-	0.33 (0)	0.32	No
	9	L5	O1 (1.10)	OT1 (0.22)	α2 (0.15)	0.43 (0)	-	0.45 (60)	0.32	Yes
	10	L7	OT2 (0.30)	α2 (0.15)	α2 (0.20)	0.30 (60)	-	0.44 (0)	0.32	No
	11	L11	O1 (1.55)	α2 (0.05)	O4 (0.25)	0.43 (0)	-	0.45 (60)	0.32	Yes
	12	-	OT1 (0.25)	O1 (1.55)	α2 (0.18)	0.22 (0)	-	0.33 (0)	0.32	No
	13	-	O1 (0.38)	α2 (0.18)	OT1 (1.45)	0.43 (0)	-	0.45 (60)	0.32	Yes
	14	-	OT1 (1.45)	O1 (0.38)	O1 (0.40)	0.22 (0)	-	0.33 (0)	0.32	No
	15	-	O1 (0.40)	OT1 (1.45)	α2 (0.15)	0.43 (0)	-	0.45 (60)	0.32	Yes
	16	-	OT1 (0.85)	α2 (0.11)	O1 (0.75)	0.22 (0)	-	0.33 (0)	0.32	No
	17	-	O1 (0.75)	OT1 (0.85)	α2 (0.11)	0.43 (0)	-	0.45 (60)	0.32	Yes
	18	-	OT1 (0.65)	α2 (0.11)	O1 (1.30)	0.22 (0)	-	0.33 (0)	0.32	No
	19	-	O1 (1.30)	OT1 (0.65)	α2 (0.30)	0.43 (0)	-	0.45 (60)	0.32	Yes
25-5	20	L1	O2 (0.70)	O2(0.07)	α2 (0.10)	0.25 (0)	-	0.25(0)	0.46	Yes
(Fig.4c)	21	L3	OT1 (0.20)	α2 (0.10)	O1 (0.34)	-	0.45	0.20(60)	0.45	Yes
	22	L4	O1 (0.34)	OT1 (0.20)	O2 (0.13)	0.43	0.18	0.43(60)	0.27	No
	23	L5	O2 (0.13)	O1 (0.34)	OT2 (0.05)	0.25(60)	-	0.25(60)	0.46	Yes
	24	L6	OT2 (0.05)	O2 (0.13)	O2 (0.24)	-	-	0.29(60)	0.37	-
	25	L7	O2 (0.24)	OT2 (0.05)	O1 (0.78)	0.25(60)	-	0.43(60)	0.46	Yes
	26	L8	O1 (0.78)	O2 (0.24)	OT1 (0.20)	0.43	0.18	0.43(60)	0.27	No
	27	L9	OT1 (0.20)	O1 (0.78)	O1 (0.30)	-	0.45	0.20(60)	0.45	Yes
	28	L10	O1 (0.30)	OT1 (0.20)	OT3 (0.38)	0.43	0.18	0.43(60)	0.27	No
	29	L12	O2 (0.60)	α2(0.38)	O1 (0.54)	0.25 (0)	0.46*	0.25(0)	0.46	Yes

* in few quantities in some areas of the corresponding lamellae

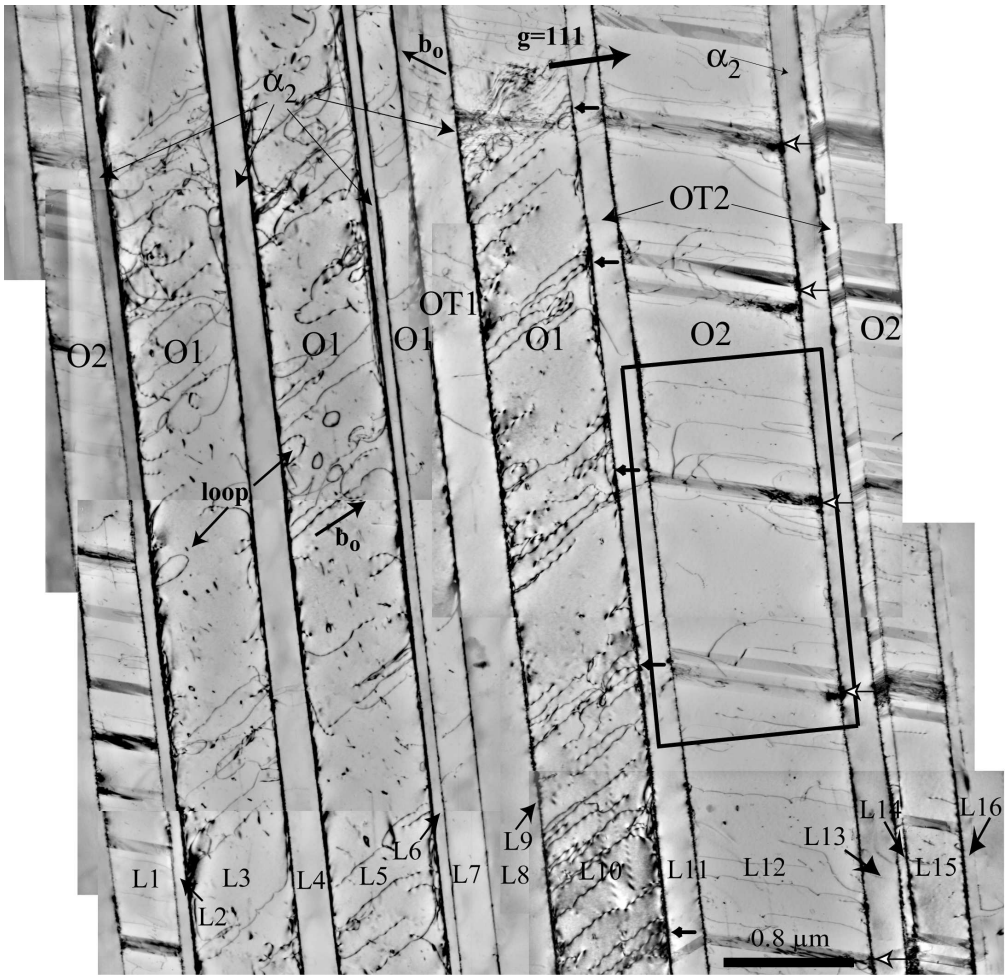

Figure 1
184x178mm (300 x 300 DPI)

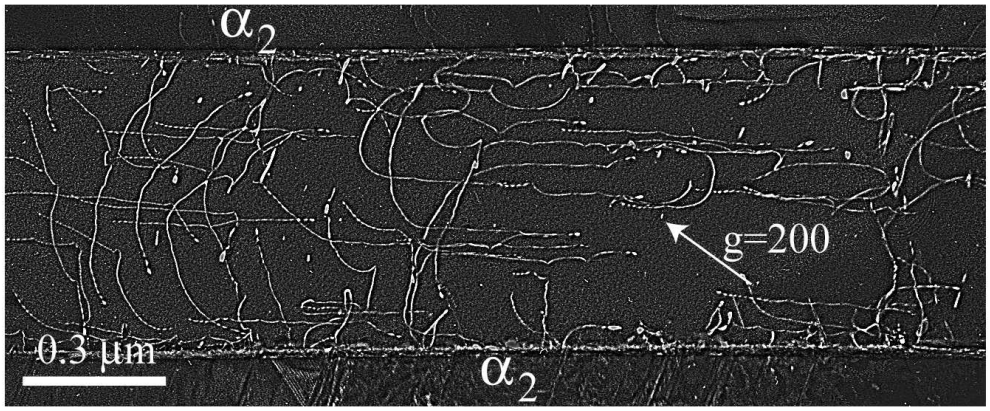

Figure 2
114x49mm (300 x 300 DPI)

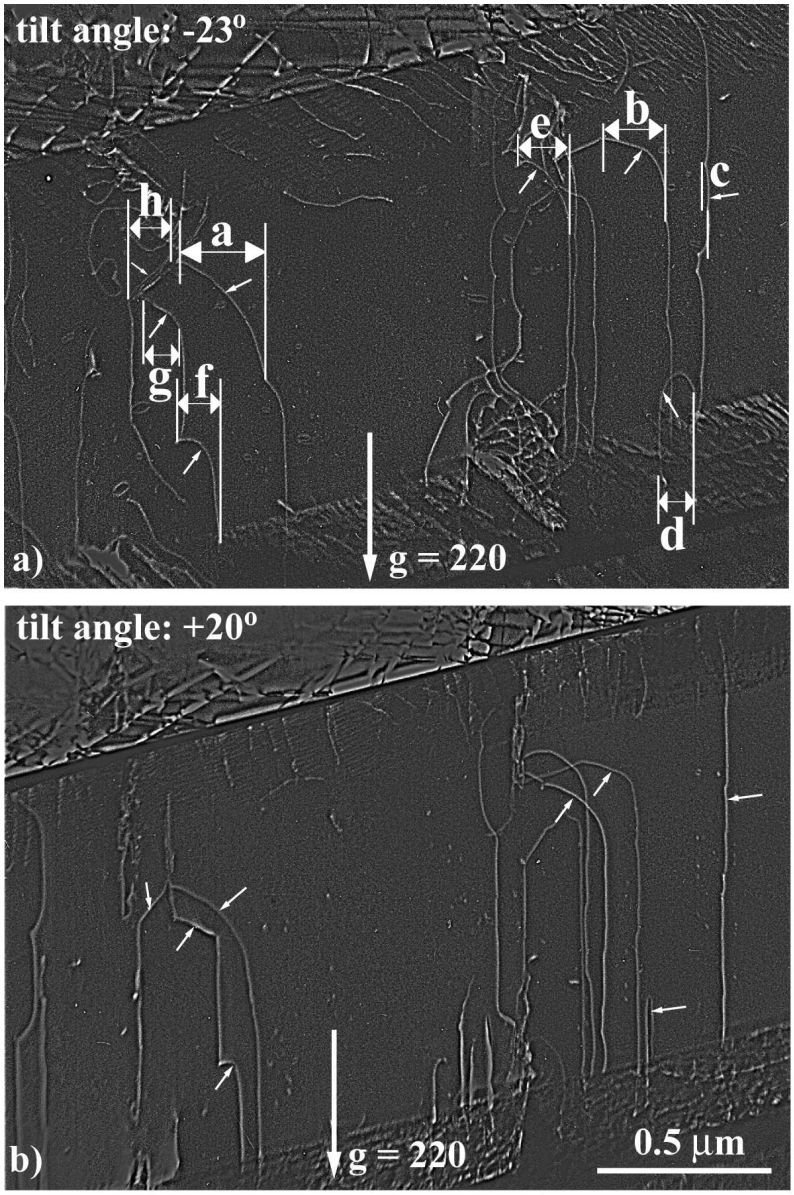

Figure 3
106x153mm (300 x 300 DPI)

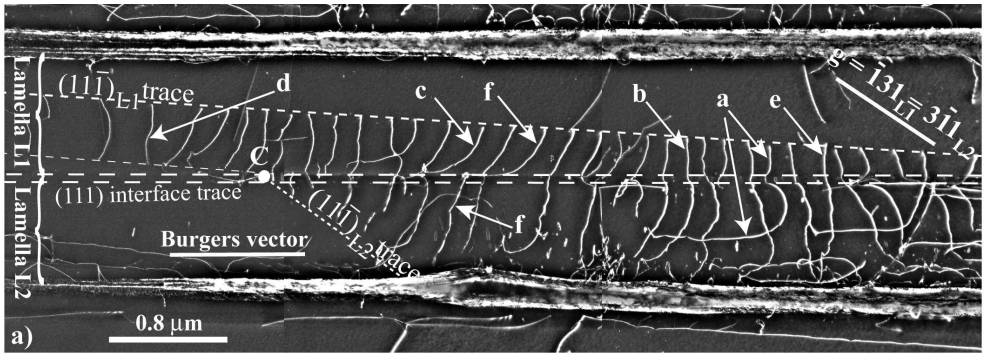

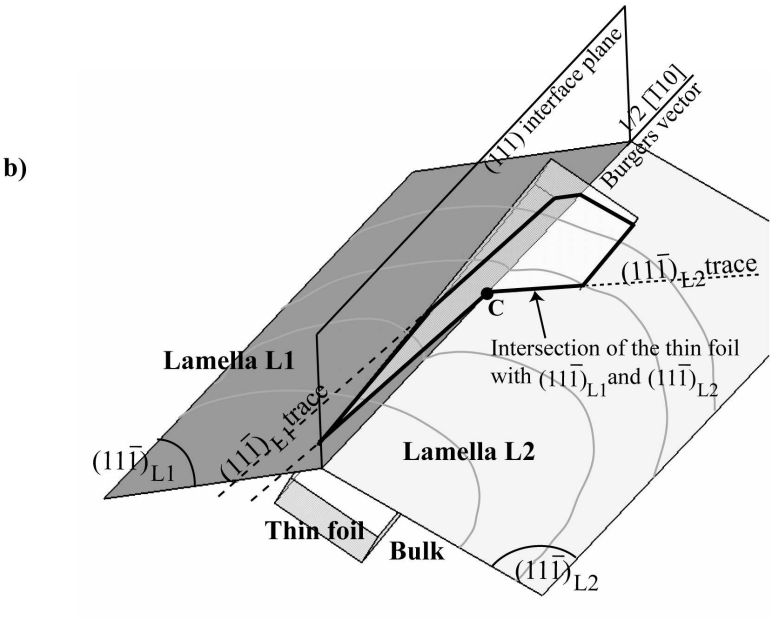

Figure 5
182x193mm (300 x 300 DPI)

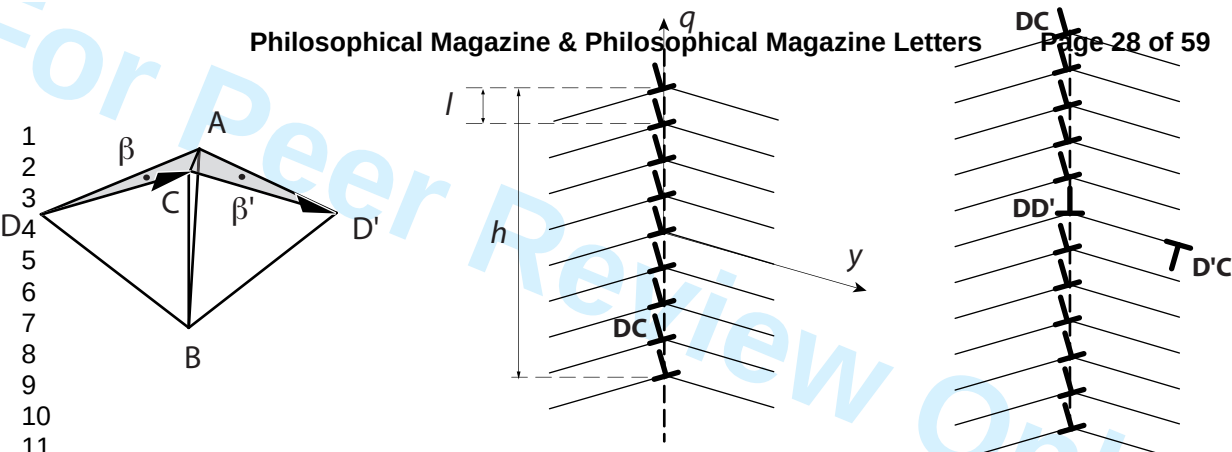

(a) (b) (c)

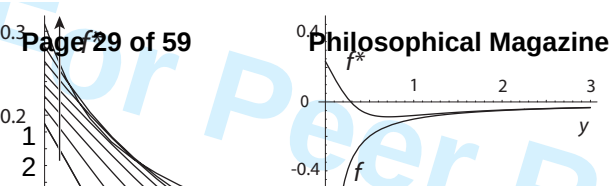

(a)

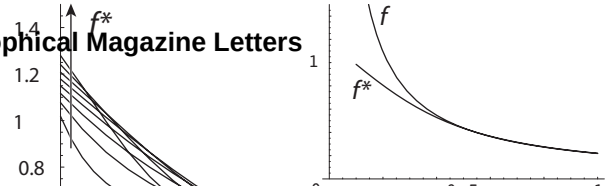

(b)

The activation and the spreading of deformation in a fully lamellar Ti-47Al-1Cr-0.2Si Alloy

J. B. Singh[a], G. Molénat[b], M. Sundararaman[a], S. Banerjee[a], G. Saada[c], P. Veyssière[c] and A. Couret[b*],

[a]*Materials Science Division, Bhabha Atomic Research Centre, Mumbai, India*
[b]*CEMES, CNRS, BP 94347, Toulouse, France*
[c]*LEM, CNRS-ONERA, BP 72, 92322 Châtillon, France*

Abstract

The spreading of deformation in a lamellar Ti-47Al-1Cr-0.2Si alloy deformed under compression is studied at 25°C and 600 °C. This microstructure is largely dominated by twin related variants which are separated by either twin interfaces or thin α_2 slabs.

The alloy deforms at both temperatures by ordinary dislocations and twins. Deformation in a particular γ variant and its adjacent twin-related variant involves the same kind of glide system, either ordinary dislocations or twins. This property is found to be true for all twin related lamellae. The occurrence of this correlated glide is explained by the introduction of the notion of "*pilot*" and "*driven*" orientations. The lamellar orientation in which the operating glide system is activated on the basis of Schmid factor considerations is termed the *pilot* orientation. It imposes its deformation system on to the twin-related lamella, called the *driven* orientation whose deformation may not involve the slip system most favoured by the applied stress.

1 INTRODUCTION

γ-TiAl-based two-phase alloys can be processed to achieve several kinds of microstructures such as fully lamellar, nearly lamellar and duplex structures. The fully lamellar microstructure exhibits improved creep strength and fracture toughness, albeit at the expense of tensile elongation properties [1]. The lamellar structure is formed when the alloy is heat-treated or hot-worked above the α transus [2, 3] followed by cooling and evolves according to the following sequence:

$$\alpha \rightarrow \alpha + \gamma \rightarrow \alpha_2 + \gamma$$

* Author for correspondence. Email: couret@cemes.fr

The microstructure is comprised of a stacking of γ ($L1_0$ structure) and α_2 ($D0_{19}$ structure) lamellae whose interfaces lie along compact planes obeying the following orientation relationships [4]:

$$\{111\}_\gamma // (0001)_{\alpha 2} \text{ and } \quad \langle 1\bar{1}0]_\gamma // \langle 11\bar{2}0\rangle_{\alpha 2}$$

The <uvw] mixed bracket notation is used in order to indicate that all permutations amongst u and v are allowed while the third index is fixed [5]. In the $L1_0$ structure, rows along the <110] directions are made of identical atoms whereas Ti and Al atoms alternate along the <101] directions. As a result, the γ-phase exhibits six different variants differing by the stacking sequence along the normal of the {111} interface (as …ABCABC… or …ACBACB…) and/or by the relative orientations of the <110] monoatomic row in the planes parallel to the interface [6]. This results in the formation of three different types of γ/γ interfaces in addition to the γ/α_2 interface in the lamellar structure. Experimentally, it is observed that the distribution of γ–variants within a grain is not random: true-twin γ/γ interface are favoured over order and pseudo-twin interfaces [7].

Compared to the γ phase, the α_2 phase is more resistant to deformation and it is generally considered that in the two-phase TiAl alloys, plasticity is restricted to the γ phase. We have recently shown that whereas some α_2 lamellae deformed at room temperature exhibit some dislocation activity, most of the transfer of plasticity across α_2 lamellae occurs by elastic shear [8]. This is why this paper addresses the plasticity of the γ phase only. We recall that in the $L1_0$ structure, dislocations with Burgers vectors 1/2<110] (the so-called "ordinary dislocations"), <011] and 1/2<112] superdislocations glide on {111} close-packed planes leaving the long-range order undisturbed as they are all unit translations of the $L1_0$ structure.

In polycrystalline two-phase TiAl alloys, the primary deformation mode is by glide of ordinary dislocations accompanied by true twinning [1,9]. It is recalled that given a {111} plane of the $L1_0$ structure, there is only one Shockley partial, i.e. $1/6\langle 11\bar{2}]$, that generates intrinsic stacking faults without first-neighbours violations. Shear in the opposite direction, $1/6\langle \bar{1}\bar{1}2]$, the anti-twinning mode, would produce extrinsic stacking faults. On the other hand, 1/6<211] Shockley partials would disturb the long-range order forming "pseudo-twins", which, as per our knowledge, have never been observed in TiAl alloys.

This paper reports on an investigation of the glide systems activated at two temperatures (25°C and 600°C), and of the factors controlling this activation in a polycrystalline lamellar TiAl alloy. The study is based on a local analysis of Schmid factors. Such questions had been

previously addressed in the case of polysynthetically twinned crystals deformed in compression as well as tension [10] and in fatigue [11], both investigations indicate the importance of the continuity of the macroscopic strain at lamellar boundaries. In the latter work, Schmid law violations have been evidenced at mismatched interfaces for the case of samples oriented in the hard mode [6], leading to the conclusion that in determining the activated deformation modes, the continuity of macroscopic strain takes over the continuity of glide planes and over Schmid factors.

2 EXPERIMENTAL PROCEDURE

2.1 Alloy preparation

Arc melted buttons of Ti-47Al-1Cr-0.2Si (expressed in atomic percentage) were kindly provided by DMMP, ONERA, Châtillon, France. The as-received buttons were homogenized at 1400°C for 3 h in a platinum furnace under flowing argon atmosphere, followed by cooling at a rate of about 15°C/min between 1400 and 900°C. The pick-up of the trace oxygen as well as moisture from the flowing gas was prevented by covering the alloy button by a thin molybdenum foil with a tungsten separator and as well as by placing a green pellet of titanium sponge in the furnace immediately before the sample in front of the incoming gas stream. This treatment was found to be sufficient to homogenize the alloy as well as to break the cast structure. The final average grain size was about 3 mm.

2.2 Mechanical tests

Compression samples with square cross-section (about 5x5x10 mm^3) were cut from the homogenized alloy by electric discharge machining (EDM). The samples were compression tested in an Instron testing machine at 25°C and 600°C at a strain rate of 3.33×10^{-4} per second. Deformation was stopped at a strain of about 2%. The 0.2% offset yield stresses for these samples were 335 and 260 MPa, respectively. It is however to be noted that, because the grain size is of the order of the sample dimension, and because various distinct deformation systems can be activated depending on Schmid factors, deformation microstructure may differ from one sample to another tested at the same temperature. The above yield-stress values are therefore subject to a significant scatter but we have checked that the above trend (i.e., the yield stress is the highest at 25°C) is unchanged.

2.3 Transmission Electron Microscopy Investigations

For transmission electron microscopy (TEM) investigations, slices of about 0.3 mm in thickness were cut by EDM at 45° and 90° to the compression face. Different directions were marked on the samples prior to cutting in order to keep track of the compression axis in the TEM foils. The slices were mechanically ground to about 0.1 mm thickness prior to being electrolytically thinned to perforation in a 6% perchloric acid and 94% butanol solution using a Fischione twin-jet electropolisher. The temperature of the electrolyte and the current were maintained at about -40°C and 20 mA, respectively. The thin foils were investigated in a JEOL 2010 transmission electron microscope at CEMES, Toulouse, France.

A number of foils were investigated by TEM. Throughout the paper, the lamellar interfaces are designated as (111). Dislocation Burgers vectors were determined by the standard **g.b** = 0 invisibility criterion. Whenever necessary, the glide plane was identified from the dependence of the apparent width of curved dislocation segments on tilt angle.

The microstructure of the undeformed alloy was characterized based on a statistical analysis of adjacent lamellae in two samples. Table 1 exemplifies this analysis on 72 contiguous lamellae comprising 52 γ and 20 α_2 lamellae whose average widths are 340 nm and 115 nm, respectively. Lamellae of the γ phase with different orientations are designated O1, O2, O3, OT1, OT2 and OT3 such that O1, O2 and O3 are in true-twin orientation with OT1, OT2 and OT3, respectively. As already reported for several lamellar TiAl alloys [12], Table 1 shows that one orientation clearly prevails (here O1) together with its twin (OT1). It is worth mentioning that the designation of the dominant lamellae may differ from one sample to another since that depends on the initial choice, which is arbitrary, made for the reference orientation.

3 RESULTS

3.1 The microstructure of the alloy deformed at 600 °C

The microstructure representative of deformation at 600°C is illustrated in figures 1 to 3. Figure 1 shows a montage including 16 lamellae labelled L1 to L16. Not clearly visible, a very thin α_2 lamella (designated L9) separates the L8 (OT1) and L10 (O1) γ-lamellae. Two types of deformation microstructures can be distinguished. The first type found in lamellae L3, L5, L7 and L10, all with orientation O1, and lamella L8 (orientation OT1), involves only ordinary dislocations all with the same Burgers vector. Although some ordinary dislocations exhibit weak contrast in the upper part of figure 1, the imaging conditions in L7 and L8 are

not good enough here to clearly show the existing microstructural similarity between these and other lamellae. The second type of microstructure, exemplified in L1, L11, L12, L14 and L15 (orientations O2 and OT2) is dominated by twins that coexist with a still significant amount of ordinary dislocations. As expected from previous investigations [8,13], α_2 lamellae exhibit very few dislocations. The above two types of deformation microstructures in γ lamellae are analyzed in the following.

3.1.1 Lamellae with ordinary dislocations

In L3, L5, L7, L8 and L10, the ordinary dislocations exhibit analogous properties and their 1/2[110] Burgers vector does not belong to the interface. They show a preference for the screw orientation and they lie in $(\bar{1}1\bar{1})$ planes inclined to the interface plane (as identified by tilt experiments). In twin-related adjacent lamellae, the Burgers vectors of the gliding ordinary dislocations (projections on plane of observation indicated by an arrow ($\mathbf{b_O}$); for O1 and OT1, see L5 and L8, respectively) are in mirror symmetry with respect to the interface. As already reported in the literature [14,15], these lamellae contain debris such as loops that attest to frequent cross-slip events. Lamellae containing ordinary dislocations with a Burgers vector at an angle to the interface plane represent the most frequent situation, though some cases of a lamella containing ordinary dislocations with Burgers vector parallel to the interface were identified (Fig.2) in another thin foil. The frequent observation of loops anchored at γ/α_2 interfaces (marked "loop" in Fig.1) indicates that emission of ordinary dislocations takes place at γ/α_2 interfaces. This property holds true whether the Burgers vector of ordinary dislocations is parallel or not to the interfaces.

3.1.2 Lamellae containing twins and associated ordinary dislocations

As mentioned earlier, twinning is the predominant mode of deformation in L1, L11, L12, L14 and L15. The twins lie on the $(\bar{1}11)$ planes of the lamellae with O2 and OT2 mirror orientations. The decrease of the twin volume fraction from L15 to L11 indicates that the twin-mediated propagation of strain has proceeded from right to left.

The area boxed in Fig.1 points to some ordinary dislocations that coexist with twins in L12 and originate from the positions where twins are in contact with the L13/L12 interface. The habit plane(s) of some portions of these dislocations ($\mathbf{b}$ = 1/2[110]) were identified by comparison between images all taken under the 220 diffraction vector parallel to the Burgers vector but under different tilt conditions. Fig. 3 shows two images of this tilt series, one with

the sample tilted by –23° (Fig. 3a) and the other tilted by +20° (Fig. 3b). The habit planes of 8 segments, namely **a**, **b**, **c**, **d**, **e**, **f**, **g** and **h**, were analysed from their apparent widths measured perpendicularly to the tilt axis. Segment **c** lie on $(\bar{1}11)$ (nearly edge-on in Fig.3b) while segment **h** is on (001). Segments **d** and **b** are in planes rather close to $(\bar{1}11)$ and (001), respectively while segments **a**, **e**, **f** and **g** lay on planes all located much closer to the (001) plane than to any of the other crystallographic planes considered in the vicinity of (001). Configurations undergoing near-(001) slip are consistent with cube slip interrupted in places by double cross-slip events. The Schmid factors (SFs) for the $1/2[110](\bar{1}11)$, $1/2[110](001)$ and $1/2[110](1\bar{1}1)$ are 0.26, 0.27 and 0.05, respectively, with the former two thus subjected to about the same shear stresses. On account of such a low Schmid factor, $1/2[110](001)$ is unlikely to have operated under the applied stress only. Rather, it is believed that the twinning partials piled-up at the L13/L14 lamellae interface did contribute significantly to the activation of this glide system. The present analysis is thus in accordance with the observation of Forwood and Gibson [16] explaining how when a twin intersects the interface along the <101] direction, ordinary dislocations are generated at γ/α_2 interfaces and glide on (001) of the lamella containing the incident twin. However, the propagation from right to left of twins suggests that these ordinary dislocations are emitted from twins impinging on the interfaces. The present observations are also consistent with the generation of ordinary dislocations where twins intersect γ/α_2 interfaces as proposed by Forwood et al. [16]. It is indeed likely that twin expansion in general and in L12 in particular, proceeds from a two-stepped mechanism : (i) transmission *per se* of a twin spearhead that occurs locally where the α_2 barrier is the weakest [16,8], (ii) then, propagation of this twin sideways. Since it is unlikely that the exact location where transmission has taken place is contained in the thin foil, one is led to conclude that the above ordinary dislocations have resulted from the impact of the interfaces by laterally expanding twins.

3.1.3 Propagation of shear across interfaces

We analyze twin propagation throughout the L15 to L11 γ–lamellae (Fig. 1). In true-twin related γ–lamellae (such as L14 and L15 in Fig. 1), mechanical twins penetrate the adjacent lamella on a plane in mirror symmetry with respect to the plane of the incident twin [17-19].

Twins nucleating at the L13/L12 γ/α_2-interface together with coexisting ordinary dislocations are arranged as if they had been activated by the internal stresses arising from the

twinning dislocations that had piled-up in the vicinity of the L14/L13 interface (see small white headed arrows in L13 on Fig. 1). The coincidence of positions of twins in L14 and L12 lamellae and a higher density of twin plates in the former indicates that the shear has been transferred from L14 to L12 lamellae through the α_2 (L13) lamella. Since hardly any dislocation contrast is observed in the L13 (α_2) lamella, it supports the hypothesis that the α_2 lamella has transmitted the shear elastically [8].

It can be seen in Fig. 1 that in L10, ordinary dislocations are preferentially localized near areas where twins have impacted the true-twin L12/L11 interface (black short arrows in lamella L11), thus suggesting that this activation of ordinary dislocations in L10 was influenced by the accumulation of stresses due to the pile-up of twinning dislocations at interfaces. The absence of a twinning activity in L11 again suggests that slip activity in L10 is simply elastically-mediated through L11 under the influence of the dislocations (twinning partials and ordinaries) locked at the L12/L11 interface.

3.2 Microstructure of the alloy deformed at 25 °C

Like samples deformed at 600°C, those deformed at room temperature exhibit twins and ordinary dislocations, as previously observed in polysynthetically twinned crystals [20] (Fig. 4). In addition, dislocations with <011] as well as 1/2<112] Burgers vector, which will not be analysed in the present paper, were also observed in places. Again, little evidence of plasticity was detected in α_2 lamellae.

3.2.1 Ordinary Dislocations

γ–lamellae deforming by ordinary dislocations, contain a uniform dislocation population reflecting homogeneous source activation at γ/α_2 interfaces and/or within the lamellae. As in the 600°C-samples, the two orientations of Burgers vectors are observed (i.e. Burgers vectors parallel or inclined to the interface) both giving rise to similar microstructural properties. Figs. 4a and 4b display representative regions where the ordinary dislocations have a Burgers vector parallel and inclined to the interface plane, respectively. They all tend to be elongated in the screw orientation although not as markedly as in the 600°C-samples conforming with previous investigations [21,22]. As the (111) interface plane is close to being edge-on in Fig. 4a, the pronounced apparent curvature indicates that part of the movement took place out of this plane, presumably in $(11\bar{1})$. The density of loops and debris is less than that observed after deformation at 600°C.

3.2.2 Twinning

Fig. 4c shows an area containing several O1 and OT1 lamellae containing a fairly homogeneous distribution of twins (the twins lying in L9 (OT1) are hardly visible because of poor contrast conditions). As in samples deformed at 600°C, twins in adjacent true-twin-related lamellae are in mirror symmetry with respect to the interface plane.

3.2.3 Crossing of twin interfaces by ordinary dislocations

Fig. 5 shows a pile-up of dislocations straddling a twin interface. The two twin-related lamellae L1 and L2 are separated by an interface inclined at about 10° to the foil normal. The pair of parallel dashed lines embodies the (111) L1/L2 interface considering that the short vertical segments are lying in the interface as explained below (see for instance the dislocation marked a). The 1/2[$\bar{1}$10] Burgers vector of the dislocations is almost parallel (4°) to the thin foil. The curvature of the dislocations indicates that they were moving from the left part to the right part of the observed area. The straight line joining the upper extremities of dislocations in L1 shows that they are piled in the $(11\bar{1})^{L1}$ plane with a marked coplanarity. In lamella L2, the lower extremities of the dislocations situated between (C) and (D) attest to glide having occurred in the $(11\bar{1})^{L2}$ plane. Schmid factors for the 1/2[$\bar{1}$10] dislocations are 0.34, 0.22 and 0.44 in (111), $(11\bar{1})^{L1}$ and $(11\bar{1})^{L2}$ planes, respectively.

The strong edge character of the dislocations of the pile-up (Fig. 5b) is a result of the thin foil surface almost parallel to the Burgers vector, which absorbs the screw portion. It should be underlined that several apparent differences in the microstructural features observed in L1 and L2 (such as the number of debris, the dislocation pinning at the neighbouring interfaces and the proportion of screw segments), originate from the fortuitous asymmetrical orientation of the thin foil with respect to the $(11\bar{1})^{L1}$ and $(11\bar{1})^{L2}$ planes (Fig. 5b). This causes certain limitations in interpreting the configuration such as in which lamella the dislocations were initially moving.

The dislocations located further on the right after mark C appear to straddle L1 and L2. Such a configuration is the result of easy cross-slip of the screw segments at the interface in agreement with similar events previously evidenced by *in situ* straining experiments [19]. Some straddling dislocations exhibit angular points or rectilinear short segments that belong to the interface (see for instance dislocations *a* or *f*). This attests to some glide having occurred in the interface plane before the transfer of these screw segments in the next lamella.

As these segments are lying in the interface, they behave as dragged portions hampering the motion of those located in the lamellae, as is illustrated by the bending of the L2 segment of dislocation *a* and of the L1 segment of dislocation *f*.

4 DISCUSSION

We have confirmed that in Ti-47Al-1Cr-0.2Si alloys compressed at 25°C and 600°C, γ lamellae are predominantly deformed either by ordinary dislocations or by twins. Ordinary dislocations are generated in the lamellae by crossing of dislocations from adjacent lamellae or as a by-product of the interaction of twins with interfaces. Emission of by-product ordinary dislocations allows for the relaxation of internal stresses, probably hampering crack formation. The process is temperature independent.

The present section is devoted to investigating the parameters pivotal to the activation of the predominant deformation mode in a given γ–lamella (§ 4.1) and to quantitatively discuss stress distribution (§ 4.2) in the specific geometry imposed in lamellar TiAl.

4.1 Factors governing slip mode activation in the driven lamellae

On the basis of Tables 2 and 3 for 600°C and room temperature samples, respectively, we analyse the role of (i) the applied stress, (ii) lamella width, and (iii) lamella environment. A number of lamellae (column 2) taken from different samples (column 1) have been analysed for the two temperatures investigated. When the lamellae referred to are taken from images presented in this paper, their labels in the corresponding figures are mentioned in column 3. Column 4 gives the orientation of the lamella analysed with its width expressed in μm in parenthesis. Columns 5 and 6 give the same information for the two adjacent lamellae, on the left-hand side (LHS) and right-hand side (RHS) respectively. Columns 7 and 8 provide the active Schmid factor (SF) for the predominant deformation mode: active SF for ordinary (ASFO) dislocations and active SF for twinning (ASFT). Columns 9 and 10 indicate the highest Schmid factor within each lamella for ordinary dislocations (HSFO) and for twinning (HSFT). In parenthesis in columns 7 and 9 is indicated the angle between the Burgers vector of the corresponding ordinary dislocations and the interface plane (0° or 60°). Finally, column 11 indicates whether the Schmid law applies within each lamella for the active deformation mode. The answer is 'Yes' in lamellae with ordinary dislocations when the ASFO is equal to the HSFO and 'No' otherwise. In order to account for experimental

uncertainties, the answer is also "Yes" when the ASFO is lower than but very close to ($\delta SF \leq -0.05$) the HSFO. The same rule is applied to twinned lamellae.

From these two tables, it appears that the lamellae with a given orientation all deform in the same way by making use of a unique slip system, i.e. only one type of ordinary dislocations or twins. Specimen 25-3 (Table 3) provides a good illustration of this property for ordinary dislocations since all 8 lamellae in the O1 orientation have deformed by the same slip system (with SF = 0.43) whereas an equivalent system of ordinary dislocations (SF = 0.45) was available. In all the investigated specimens, this property is valid *regardless of lamellar thickness*, thus ruling out the lamella width as pertinent parameters in controlling the slip system activation.

Tables 2 and 3 also illustrate that two twin-related lamellae (i.e. O_i and OT_i) exhibit the same predominant deformation mode *whether they are adjacent or separated by an α_2 lamella*. That is the case for ordinary dislocations in lamellae 2 to 6, 22 to 24, 26 to 28 in Table 2 and 2 to 4, 5 to 19 (except 10-OT2) in Table 3 and for twins in lamellae 7 to 12 and 14 to 21 in Table 2; 21-22, 26 to 29 in Table 3. Figure 1 provides a fair illustration of these properties.

The following sections are aimed at explaining why twin-related lamellae deform by the same predominant mode.

4.1.1 Ordinary dislocations

Tables 2 and 3 show that out of the two possible orientations of 1/2<110] Burgers vectors (parallel or inclined to the interface plane), one only operates in twin-related adjacent variants. For a Burgers vector parallel to the interface, this property is illustrated by lamellae 26 to 28 of sample 600-3 (table 2), lamellae 1 to 4 of sample 25-1 (table 3) and lamellae 5 to 18 (except 10-OT2) of sample 25-3 (table 3). For a Burgers vector at 60° to the interface, this is seen in the case of lamellae 2 to 6 of sample 600-1 (table 2) and lamellae 22 to 24 of sample 600-2 (table 2). It is worth noting that when in a variant O_i (i = 1 to 3) the Schmid law applies (i.e., $ASFO^{Oi} = HSFO^{Oi}$), then in the conjugate OT_i variant it may (samples 600-3 and 25-1: $ASFO^{OTi} = HSFO^{OTi}$) or not (samples 600-1, 600-2 and 25-3: $ASFO^{OTi} < HSFO^{OTi}$) apply.

A scenario based on the notion of "*pilot*" and "*driven*" orientations explains how a given glide system of ordinary dislocations becomes the only operative system within O_i/OT_i twin-related variants. In this scenario, the O_i orientation that is capable of imposing the operation of given ordinary system in the OT_i orientation is referred to as the *pilot* orientation while the

OT_i orientation itself is called the *driven* orientation. Sources of ordinary dislocations are activated within the lamellae with an O_i orientation, in consistency with the Schmid law ($ASFO^{pilot} = HSFO^{pilot}$ and $ASFO^{pilot} \geq HSFO^{driven}$ of the OT_i conjugate orientation). In other words, the pilot orientation imposes the slip system operating in the twin related conjugate variants, irrespective of the Schmid factor of the latter. The operating Burgers vector may either be inclined to the interface plane (Fig.1 and Fig.4b) or parallel to it (Fig.2 and Fig.4a). Fig. 1 shows this scenario taking place between orientation O1 (lamellae L3, L5, L7, L10) and orientation OT1 (lamella L8) acting as the pilot orientation (ASFO = 0.49) and the driven orientation (ASFO = 0.28 when HSFO = 0.39 is available), respectively. One extreme case is provided by sample 600-2 where the OT2 pilot orientation (lamella 23) imposes a glide system in the O2 driven orientation (lamella 22) with a very unfavourable resolved shear stress (ASFO = 0.04 when HSFO = 0.31 is available). The property that the Schmid factor is instrumental in determining which orientation can act as pilot orientation is found to be independent of the volume fraction of the different variants. This, however, cannot be concluded for certain since slip transfer may not have been initiated in the region observed by TEM but elsewhere the relative abundance of the twin-oriented lamellae is reversed (Pilot > Driven).

Situations of a violation of the Schmid law similar to that exhibited by lamella L7 in sample 25-3 can be encountered too (Fig. 4a). In such a case of not twin related interfaces, Nakano and co-workers [11] have evidenced a similar violation of the Schmid law. They have concluded that the predominant factor in selecting the operative systems is the continuity of macroscopic strains, which imposes that the resultant Burgers vector of the emitted dislocations be parallel and equal in magnitude to that of the incident dislocations (see, however, § 4.3).

Ordinary dislocations having a Burgers vector parallel to the interface cross through interfaces by a simple cross-slip process as illustrated in Fig. 5. Hence no problem is expected for such a transmission from the pilot to the driven orientation. The transmission of an ordinary dislocation whose Burgers vector is at 60° from the interface (e.g. lamellae 2 to 6 in sample 600-1 and 22 to 24 in sample 600-2) is, however, not as easy as reported by Zghal and co workers [19]. They actually reported *in situ* observations of such dislocations impacting an interface between twin-related variants. No transfer at all occurred in this case. In the vicinity of the interface and within the OT_i lamella, these authors nevertheless observed one case of the operation of a source of ordinary dislocations with a Burgers vector lying at 60° from the interface. The observation was interpreted as resulting from the built up of

internal stresses by accumulation of incident dislocations, which is fully supported by the present post-mortem observations.

4.1.2 Twinning mode

Similar situations of a *pilot*/*driven* pair have been encountered for twinning. This is exemplified by sample 25-5 (Table 3) where orientation OT1 is pilot since $ASFT^{pilot} = HSFT^{pilot}$ whereas O1 is the driven variant ($ASFT^{driven} < HSFT^{driven}$). At least in the area shown in Fig. 4c, it is worth noting that the volume fraction occupied by the pilot orientation is lower than that covered by the driven orientation. Samples 600-1 (lamellae numbers 7-12) and 600-2 (lamellae numbers 14 to 21) are representative of another situation in which the *pilot/driven* concept applies in a slightly different manner. In these last two cases and for the twin-related orientations the ASFT is always that of highest Schmid factor for twinning (HSFT). The Schmid law for twinning is therefore never violated. However, as exemplified by sample 600-1, in the OT2 orientation, the Schmid factor available for ordinary dislocations (HSFO = 0.46) is clearly higher than that for the active twin dislocations (ASFT = 0.18).

Twins thus appear to be preferentially generated in lamellae with the O_i pilot orientation and then expand in the OT_i oriented lamellae by emission from the O_i/OT_i interface of twins in the {111} mirror planes of the O_i twin plane as already observed in several studies [17,18,19]. Fig. 1 also illustrates the situation for twinning with the O2 orientation (lamellae L12 and L15) and OT2 orientation (lamellae L11 and L14) acting as the pilot and the driven orientations, respectively.

4.1.3 A global description of deformation in the lamellar structure

The spreading of strain in the lamellar microstructure requires the crossing of coherent (twin) and mismatched (ordered domains or pseudo-twin) interfaces as well as the propagation of deformation through α_2 slabs. As far as the α_2 lamellae are concerned, it has been recently proposed that strain transfer occurs mainly through the effect of elastic strain field, which activate sources in neighbouring lamellae [8]. In the case of mismatched interfaces Schmid law is often violated. In those cases geometrical factors such as the conservation of the Burgers vectors and the continuity of glide/twin planes are likely to be more critical [10,19,23] in addition to internal stress concentrations due to dislocation pile-ups.

At twin-related interfaces, deformation is transferred through the activation of a conjugate deformation system, with the slip systems of the operating dislocations in mirror symmetry. In fact, the factor predominant in deformation transfer at coherent twin interfaces appears to be the continuity of the glide/twin planes. On the other hand, except for the easy case of ordinary dislocations with Burgers vectors parallel to the interface plane for which crossing occurs by a simple cross-slip, the sum of the Burgers vectors of incident dislocations is not equal to that of the emitted dislocations. In other words, the condition of strain continuity proposed by [10,11] is not obeyed locally at twin interfaces and this suggests an additional effect of internal stresses.

One should keep in mind that the distribution of lamellae is not random. It is actually generated as a result of several transformations that are activated at different temperatures during heat treatment [24]. The high temperature transformation produces wide γ lamellae with a unique orientation. Transformations operating at lower temperatures, above and below the eutecticoid temperature, generate thin lamellae which are twin-related to the existing wide lamellae. In polycrystalline TiAl alloys, this results in a lamellar microstructure dominated by two twin-related orientation variants [7,12]. Clearly, it is this prevalence of adjacent-twin related lamellae in the microstructure that confers the analysis of strain transfer between pilot-driven, adjacent twin-related orientations its full importance.

In summary, deformation is activated in the pilot lamellae in which the activation of either ordinary dislocations or of twins is encouraged by adequate Schmid factors and resolved shear stresses, and these dislocations subsequently invade the driven orientation OT_i, in the twin-related variant.

4.2 Stress transfer

This section summarizes the main results of a theoretical analysis of the conditions under which dislocations can be expelled from the interface into the twin-oriented driven lamella, assuming that at the origin of slip transmission is a finite ensemble of equidistant pilot dislocations blocked at the interface. The account made here is essentially concerned with ordinary dislocations with a Burgers vector inclined to the interface in which case slip transmission can be accompanied by a violation of the Schmid law. Some results concerning twinning dislocations will be briefly summarized too. A full account of this model will be the object of a forthcoming paper.

4.2.1 Slip transfer involving inclined ordinary dislocations

The situation observed experimentally is represented by ordinary dislocations with Burgers vectors **DC** and **D'C** gliding on ADC and AD'C mirror planes on the pilot and the driven lamellae, respectively (Fig. 6(a); ABC is the interface plane). On the one hand, an infinite wall of equidistant dislocations whose Burgers vector **DC** is inclined to the interface would generate a long-range stress field in the twin-oriented lamella. Created at **DC** dislocations of the wall, **D'C** dislocations would leave interfacial edge dislocations with Burgers vector **DD'** (i.e. **DD'** = **DC** - **D'C**) engendering a low angle tilt boundary. **D'C** dislocations can thus be thought of as being repelled by the boundary generating in the driven lamella a deformation compatible with that of the pilot and relaxing the internal long-range stresses. A similar reasoning applies, of course, to **CD'** dislocations gliding towards the interface. On the other hand, the interaction between a single pilot **DC** dislocation and a **D'C** dislocation is attractive hindering emission in the latter lamella. Emission would be similarly impeded in case of a pile-up of pilot dislocations. The properties of a finite array of interfacial pilot dislocations are somewhat intermediate between those of a single dislocation and of an infinite array. One indeed expects that, when the driven dislocations are close to the finite array, the force that the latter exerts on driven dislocations is repulsive, akin to that of an infinite array, whereas it is attractive, akin to that of a single dislocation at large distances from the array.

Consider a finite array of height h of interfacial, equidistant **DC** dislocations. The force d**F*** it exerts on a driven dislocation can be calculated considering the array as an homogenous distribution of infinitesimal dislocations with Burgers vector

$$\mathrm{d}\mathbf{b} = g\,\mathbf{b}\,\mathrm{d}X \tag{1a}$$

where $g = l^{-1}$ is the reciprocal of the dislocation repeat distance. Integrated over the entire array, the projection df* of d**F*** in the glide direction, assumes the following form

$$f^*(y,q) = \mu g b^2 \varphi(y,q) \tag{2a}$$

where the distances y and q in the driven slip plane and in the interface, respectively are given in units of h. At large distances from the interface the force becomes

$$f^*(y,0) \approx \mu g b^2 \frac{\alpha}{y} \tag{2b}$$

where α is a factor that depends on the geometry of the interaction under consideration and on the Poisson's ratio ($\nu = 1/3$). Given b, g and y, the modulus of α represents the strength of the interaction between the pilot and driven dislocations, which is itself at the origin of slip transmission. The coefficient α is negative ($\alpha = -0.1$). In the case of a single pilot dislocation, the interaction far from the array force is written

$$f = \frac{\alpha\, \mu b^2}{hy} \tag{3}$$

Expression (2b) that can be rewritten as

$$f^*(y,0) = ghf \tag{4}$$

states that at large distances from the array the stress exerted on the driven dislocation is that of a dislocation with Burgers vector *nb*, as is expected. The force *f** (expression (2a)) is plotted in Figure 7(a) versus *y* for various values of *q*. It is seen that, the force is a maximum near the interface ($y \approx 0$). The stress, which is actually large enough to nucleate plastic strain, does not vary significantly within a band of thickness 0.8 *h*. The repulsive effect is the most pronounced in the upper part of the driven lamella. The inset in Figure 7(a) illustrates how the force *f** exerted by the array changes its sign at a certain distance from the interface. It shows in addition that the agreement between *f** and *f* is good at long distances from the interface.

4.2.2 Twinning

The above equations (3) and (4) remain valid and the same reasoning applies in the case of homogeneous twinning regarded as resulting from Shockley dislocations $\beta\mathbf{A}$ and $\beta'\mathbf{A}$ gliding in the pilot and in the driven lamellae, respectively. Here, gb_t is a fixed quantity amounting to 2/3, and the force does not change sign. Remarkably, the coefficient α ($=0.22$) is positive and twice as large as in the above case of slip transmission by perfect dislocations. Figure 7(b) shows that the force is almost uniform across the band section, and that its repulsive effects are manifested at distances comparatively larger than those calculated for a band of perfect dislocations of equal thickness (Figure 7(a)).

In summary, these calculations show that whereas neither a single dislocation nor an infinite dislocation array can generate a stress field adequate to ordinary dislocation emission, a band of finite height can provide the required stress field hence giving rise to a Schmid law violation (e.g. sample 600-1 sample, Figure 1 and Table 2). Beside, the stress field produced by a twin is shown to be favorable to twin emission in a mirror plane (e.g. sample 600-1 and 25-5 samples in Figures 1 and 4c, respectively).

5 CONCLUSIONS

The main results of the present investigation of the deformation systems activated during deformation at 25° and 600°C in a fully lamellar TiAl alloys can be summarized as follows:

- Strain is mainly accommodated by twins and ordinary dislocations.
- In a given lamella, the deformation microstructure is mostly dominated by one system. Secondary systems are seldom activated as the result of interaction between twins and interfaces.
- In a given grain, the members of a given variant family all deform by means of the same slip system regardless of their neighbouring lamellae and of the lamella thickness.
- Deformation is first initiated in a lamellae orientation, termed as the *pilot*, on the basis of Schmid factor considerations. That is true for lamellae deforming by ordinary dislocations as well for lamellae deforming by twinning.
- The deformation mode in adjacent, twin-related variants, the *driven* orientation, is dictated by that of the *pilot* orientation. When deformation occurs by ordinary dislocations, the system activated in the driven orientation is symmetrical to that activated in the pilot orientation. In the case of twinning, twins are emitted in plane in mirror symmetry to the plane of incident twins.
- The continuity of glide/twin planes determines the activated systems in the driven orientation.
- Slip transfer across twin-oriented lamellae necessitates that the interfaces be impacted by slip bands with a finite thickness.

The importance of the pilot/driven mechanism stems from the fact that the lamellar microstructure is largely dominated by two twin-related orientations.

Acknowledgements

The authors acknowledge the Indo-French Centre for the Promotion of Advanced Research, New Delhi for sponsoring this project (No. 2308-3) and for funding the visit of one of the authors (J.B.S.) to Toulouse, France. The authors wish to thank Drs Shigehisa Naka and Marc Thomas of DMMP/ONERA for kindly provide the material and Dr. Rajeev Kapoor of Materials Science Division, B.A.R.C., for his help to carry out deformation experiments.

REFERENCES

[1] APPEL, F., and WAGNER, R., 1998, *Mater. Sci. Eng.*, **R22**, 187.

[2] WILLEY, L.A., and MARGOLIN, H., 1973, *Metals Handbook*, ASM, Metal Park, OH, 8th Edition, vol. 8, p.264.

[3] KIM, Y.-W., 1991, *Microstructure/Property Relationships in Titanium Aluminides and Alloys*, edited by Y.-W. Kim and R.R. Boyer (TMS Warrendale, PA), p. 91.

[4] BLACKBURN, M. J., 1970, *The Science, Technology and Applications of Titanium*, edited by R. Jaffe and N. Promisel (Oxford: Pergamon), p. 633.

[5] HUG, G., LOISEAU, A., and VEYSSIÈRE, P., 1988, *Phil. Mag. A*, **57**, 499.

[6] FUJIWARA, T, NAKAMURA, A., HOSOMI M., NISHITANI, S.R., SHIRAI, Y., YAMAGUCHI Phil. Mag A 1990;61(4):591.

[7] ZGHAL, S., NAKA, S., and COURET, A., 1997, *Acta metall. mater*., 45, 3005.

[8] SINGH, J.B., MOLENAT, G., SUNDARARAMAN, M., BANERJEE, S., SAADA, G., VEYSSIÈRE, P., COURET, A., Submitted to Phil. Mag. letters.

[9] FARENC, S., COUJOU, A., and COURET, A., 1993, *Phil. Mag. A*, 67, 127

[10] KISHIDA, K., INUI, H., and YAMAGUCHI, M., 1998, *Phil. Mag.* A, **78**, 1.

[11] NAKANO T, BIERMANN H, RIEMER M, MUGHRABI H, NAKAI Y, UMAKOSHI Y. Phil. Mag A 2001;81(6):1447

[12] ZGHAL, S., THOMAS, M., NAKA, S., and COURET, A., 2001c, *Phil. Mag.* Letters, 81, 537.

[13] APPEL F, BEAVEN PA,WAGNER R., Acta metal. mater. 1993;41:1721

[14] VIGUIER, B., HEMKER, K.J., BONNEVILLE, J., LOUCHET, F., and MARTIN, J.L., 1995, *Phil. Mag. A.*, **71**, 1295.

[15] SRIRAM, S., DIMIDUK, D.N., HAZZELDINE, P.M., and VASUDEVAN, V.K., 1997, *Phil. Mag. A.*, **76**, 965.

[16] FORWOOD, C.T., and GIBSON, M.A., 2000, *Phil. Mag. A*, 80, 2785

[17] WIEZOREK, J.M.K., ZHANG, X.D., MILLS, M.J., and FRASER, H.L., 1998, *Phil. Mag. A*, **78**, 217.

[18] GIBSON, M.A., and FORWOOD, C.T.,2000, *Phil. Mag. A*, 80, 2747

[19] ZGHAL, S., and COURET, A., 2001, *Phil. Mag.* A, 81,365.

[20] INUI, H., NAKAMURA, A., OH, M. H., and YAMAGUCHI, M., 1992, *Phil. Mag.* A, **66**, 557.

[21] GRÉGORI, F., 1999, PhD Thesis, University of Paris VI, France

[22] GRÉGORI, F. and P. VEYSSIÈRE, *Gamma Titanium Aluminides*, Y.-W. Kim, D.M. Dimiduk, and M.H. Loretto, Editors. 1999, Minerals, Metals & Materials Society: Warrendale. p. 75-82.

[23] ZGHAL, S., COUJOU, A., and COURET, A., 2001, *Phil. Mag.* A, 81, 345.

[24] ZGHAL, S., THOMAS, M., NAKA, S., FINEL, A., COURET, A., Acta metal. mater. 2005;53:2653.

Figure captions

Fig.1. A montage of bright-field (BF) images taken from the 600-1 sample (L1, L3, L5, L7, L8, L10, L11, L12, L14 and L15 are γ lamellae and L2, L4, L6, L9, L13 and L16 are α_2 lamellae). The projected Burgers vectors of ordinary dislocations within O1 and OT1 orientation are shown by arrow as $\boldsymbol{b_0}$ in L5 and L8. A detailed view of the boxed region is given in Fig. 3. The microstructural similarity between L7 and L8 on the one hand and L3, L5, L10 on the other is visible in the upper part on the figure.

Fig.2. A weak-beam micrograph of ordinary dislocations in a γ–lamellae (sample 600-3). The Burgers vector is parallel to the interface plane.

Fig.3. Weak-beam identification of planes containing dislocations of the boxed area of Fig. 1 (L12). Examples at tilt angles θ = -23° and θ = 20°). **g** = 220. The habit planes of segments **a** to **h** have been identified (see text for details).

Fig.4. Samples deformed at room temperature. (a) A montage of images from the 25-3 sample showing ordinary screw dislocations with Burgers vector parallel to the interface plane. (b) BF image of a γ–lamella containing ordinary dislocations whose Burgers vector is inclined to the interface plane (sample 25-4). (c) Deformation by twinning (25-5 sample).

Fig.5. (a) DF image showing ordinary dislocations straddling a twin interface. (b) 3D schematic drawing based on TEM analysis.

Fig.6. The crystallography of slip transmission used in the calculations. (a) The two twin-related Thompson tetrahedral. ADC and AD'C are the pilot and driven slip planes, and ABC is the twin interface. (b) Pilot dislocations have accumulated at the interface forming an array of equidistant **DC** dislocations. (c) A **D'C** dislocation escapes from an infinite interface leaving an edge **DD'** dislocation with a Burgers vector normal to the interface.

Fig.7. Plot of the force f^* versus y, the distance of the driven dislocations from the interface in the slip direction (in units of h) for various values of q (see Figure 5b)). (a) The transmission of perfect dislocations. From bottom to top, the arrow intersects the curves corresponding to q = -0.4, -.03, -0.2, (-0.1 and 0), 0.1, 0.2, 0.3 0.4. (b) The transmission of partial dislocations (twinning). From bottom to top, the arrow intersects the curves corresponding to y = -0.4, -.03, -0.2, (-0.1 and 0), 0.1, 0.2, 0.3 0.4. The inset in (b) is similar to that of (a). The insets compare, as a function of y, the force exerted onto a driven dislocation by an array (thickness h), force f^*, and by a single pilot dislocation, force f.

Table caption

Table 1. Quantitative description of the two-phase microstructure investigated..

Table 2. Summary of the general features and of the deformation modes of the γ lamellae in samples compressed at 600° C.

Table 3. Summary of the general features and of the deformation modes of the γ lamellae in samples compressed at 25° C.

Table 1.

Volume Fractions (%)						
α_2	**γ Matrix**			**γ Twins**		
0.12	0.76			0.12		
	O1	**O2**	**O3**	**OT1**	**OT2**	**OT3**
	0.82	0.07	0.11	0.69	0.30	0.01
Distribution of different γ/α_2 and γ/γ interfaces (%)						
γ/α_2 interfaces	**γ/γ interfaces**					
55	45					
	Ordered domain		**Twin**		**Pseudo-twin**	
	40		40		20	

6 Table 2

Sample id	Lamella No.	Lamellae		OR of Bounding Lamellae		Schmid factors for the activated systems		Highest Schmid factors available		Schmid Law
		id	OR	L.H.S.	R.H.S.	ASFO	ASFT	HSFO	HSFT	
600-1	1	L1	O2 (0.36)	α2 (-)	α2 (0.08)	-	0.38	0.30 (0)	0.39	Yes
(Fig; 1)	2	L3	O1 (0.64)	α2 (0.08)	α2 (0.18)	0.49 (60)	-	0.49 (60)	0.19	Yes
	3	L5	O1 (0.66)	α2 (0.18)	α2 (0.07)	0.49 (60)	-	0.49 (60)	0.19	Yes
	4	L7	O1 (0.23)	α2 (0.07)	OT1 (0.37)	0.49 (60)	-	0.49 (60)	0.19	Yes
	5	L8	OT1 (0.36)	O1 (0.23)	α2 (0.00)	0.28 (60)	-	0.39 (0)	0.31	No
	6	L10	O1 (0.70)	α2 (0.00)	OT2 (0.22)	0.49 (60)	-	0.49 (60)	0.19	Yes
	7	L11	OT2 (0.22)	O1 (0.70)	O2 (1.00)	-	0.18	0.46 (60)	0.18	Yes
	8	L12	O2 (1.00)	OT2 (0.22)	α2 (0.22)	-	0.38	0.30 (0)	0.39	Yes
	9	L14	OT2 (0.08)	α2 (0.22)	O2 (0.36)	-	0.18	0.46 (60)	0.18	Yes
	10	L15	O2 (0.36)	OT2 (0.08)	α2 (0.08)	-	0.38	0.30 (0)	0.39	Yes
	11	-	OT2 (0.17)	OT1 (0.12)	O2 (0.60)	-	0.18	0.46 (60)	0.18	Yes
	12	-	O2 (0.60)	OT2 (0.17)	O1 (0.27)	-	0.38	0.30 (0)	0.39	Yes
	13	-	O1 (0.27)	O2 (0.60)	OT1 (0.13)	0.49 (60)	-	0.49 (60)	0.19	Yes
600-2	14	-	O1 (0.11)	α2 (0.06)	OT1 (0.05)	-	0.40	0.33 (0)	0.40	Yes
	15	-	OT1 (0.05)	O1 (0.11)	O1 (0.04)	-	0.34	0.38 (0)	0.34	Yes
	16	-	O1 (0.04)	OT1 (0.05)	α2 (0.00)	-	0.40	0.33 (0)	0.40	Yes
	17	-	O1(0.83)	α2 (0.00)	α2 (0.52)	-	0.40	0.33 (0)	0.40	Yes
	18	-	OT1 (0.03)	α2 (0.52)	O1 (0.02)	-	0.34	0.38 (0)	0.34	Yes
	19	-	O1 (0.02)	OT1 (0.03)	OT1 (0.06)	-	0.40	0.33 (0)	0.40	Yes
	20	-	OT1 (0.06)	O1 (0.02)	O1 (0.00)	-	0.34	0.38 (0)	0.34	Yes
	21	-	OT1 (0.16)	O1 (0.00)	O1 (0.00)	-	0.34	0.38 (0)	0.34	Yes
	22	-	O2 (0.25)	α2 (0.08)	OT2 (0.10)	0.04 (60)	-	0.31 (0)	0.25	No
	23	-	OT2 (0.10)	O2 (0.25)	α2 (0.06)	0.48 (60)	-	0.48 (60)	0.48	Yes
	24	-	OT2 (0.58)	α2 (0.06)	α2 (0.00)	0.48 (60)	-	0.48 (60)	0.48	Yes
600-3	25		O1 (0.67)	O2 (0.15)	α2 (0.03)	0.39 (0)	-	0.39 (0)	0.41	Yes
(Fig.2)	26	-	O3 (0.51)	O1 (0.57)	O6 (0.03)	0.44 (0)	-	0.49 (60)	0.32	Yes
	27	-	OT3 (0.03)	O3 (0.51)	O3 (0.31)	0.29 (0)	-	0.29 (0)	0.34	Yes
	28	-	O3 (0.31)	OT3 (0.03)	α2 (0.02)	0.44 (0)	-	0.49 (60)	0.32	Yes

Table 3

Sample id	Lamella No.	Lamellae		OR of Bounding Lamellae		Schmid factors for the activated systems		Highest Schmid factors available		Schmid Law
		id	OR	L.H.S.	R.H.S.	ASFO	ASFT	HSFO	HSFT	
25-1	1	-	O1 (0.70)	OT2 (0.38)	α2 (0.42)	0.49 (0)	-	0.49 (0)	0.21	Yes
	2	-	O1 (1.17)	α2 (0.42)	OT1 (0.11)	0.49 (0)	-	0.49 (0)	0.21	Yes
	3	-	OT1 (0.11)	O1 (1.17)	O1 (0.88)	0.44 (0)		0.44 (0)	0.21	Yes
	4	-	O1 (0.88)	OT2 (0.38)	α2 (0.42)	0.49 (0)	-	0.49 (0)	0.21	Yes
25-3	5	-	OT1 (0.12)	α2 (0.25)	O1 (0.60)	0.22 (0)	-	0.33 (0)	0.32	No
(Fig.4a)	6	L1	O1 (0.60)	OT1 (0.12)	α2 (0.05)	0.43 (0)	-	0.45 (60)	0.32	Yes
	7	L3	O1 (0.85)	α2 (0.05)	O4 (0.22)	0.43 (0)	-	0.45 (60)	0.32	Yes
	8	L4	OT1 (0.22)	O1 (0.85)	O1 (1.12)	0.22 (0)	-	0.33 (0)	0.32	No
	9	L5	O1 (1.10)	OT1 (0.22)	α2 (0.15)	0.43 (0)	-	0.45 (60)	0.32	Yes
	10	L7	OT2 (0.30)	α2 (0.15)	α2 (0.20)	0.30 (60)	-	0.44 (0)	0.32	No
	11	L11	O1 (1.55)	α2 (0.05)	O4 (0.25)	0.43 (0)	-	0.45 (60)	0.32	Yes
	12	-	OT1 (0.25)	O1 (1.55)	α2 (0.18)	0.22 (0)	-	0.33 (0)	0.32	No
	13	-	O1 (0.38)	α2 (0.18)	OT1 (1.45)	0.43 (0)	-	0.45 (60)	0.32	Yes
	14	-	OT1 (1.45)	O1 (0.38)	O1 (0.40)	0.22 (0)	-	0.33 (0)	0.32	No
	15	-	O1 (0.40)	OT1 (1.45)	α2 (0.15)	0.43 (0)	-	0.45 (60)	0.32	Yes
	16	-	OT1 (0.85)	α2 (0.11)	O1 (0.75)	0.22 (0)	-	0.33 (0)	0.32	No
	17	-	O1 (0.75)	OT1 (0.85)	α2 (0.11)	0.43 (0)	-	0.45 (60)	0.32	Yes
	18	-	OT1 (0.65)	α2 (0.11)	O1 (1.30)	0.22 (0)	-	0.33 (0)	0.32	No
	19	-	O1 (1.30)	OT1 (0.65)	α2 (0.30)	0.43 (0)	-	0.45 (60)	0.32	Yes
25-5	20	L1	O2 (0.70)	O2(0.07)	α2 (0.10)	0.25 (0)	-	0.25(0)	0.46	Yes
(Fig.4c)	21	L3	OT1 (0.20)	α2 (0.10)	O1 (0.34)	-	0.45	0.20(60)	0.45	Yes
	22	L4	O1 (0.34)	OT1 (0.20)	O2 (0.13)	0.43	0.18	0.43(60)	0.27	No
	23	L5	O2 (0.13)	O1 (0.34)	OT2 (0.05)	0.25(60)	-	0.25(60)	0.46	Yes
	24	L6	OT2 (0.05)	O2 (0.13)	O2 (0.24)	-	-	0.29(60)	0.37	-
	25	L7	O2 (0.24)	OT2 (0.05)	O1 (0.78)	0.25(60)	-	0.43(60)	0.46	Yes
	26	L8	O1 (0.78)	O2 (0.24)	OT1 (0.20)	0.43	0.18	0.43(60)	0.27	No
	27	L9	OT1 (0.20)	O1 (0.78)	O1 (0.30)	-	0.45	0.20(60)	0.45	Yes
	28	L10	O1 (0.30)	OT1 (0.20)	OT3 (0.38)	0.43	0.18	0.43(60)	0.27	No
	29	L12	O2 (0.60)	α2(0.38)	O1 (0.54)	0.25 (0)	0.46*	0.25(0)	0.46	Yes

* in few quantities in some areas of the corresponding lamellae

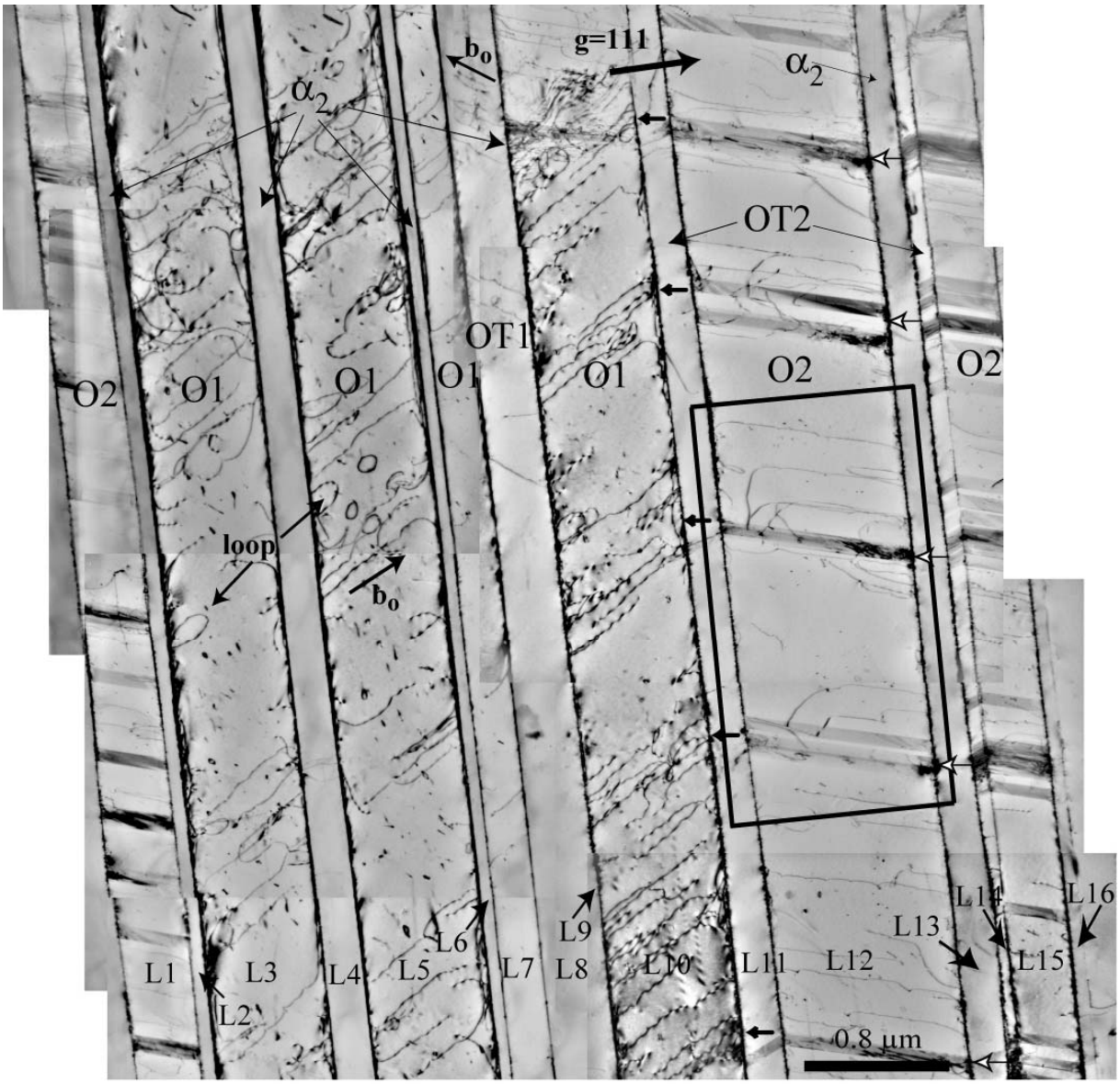
b0
g=111
α2
α2
OT2
OT1
O2
O1
O1
O1
O1
O2
O2
loop
b0
L1
L2
L3
L4
L5
L6
L7
L8
L9
L10
L11
L12
L13
L14
L15
L16
0.8 μm

Figure 1

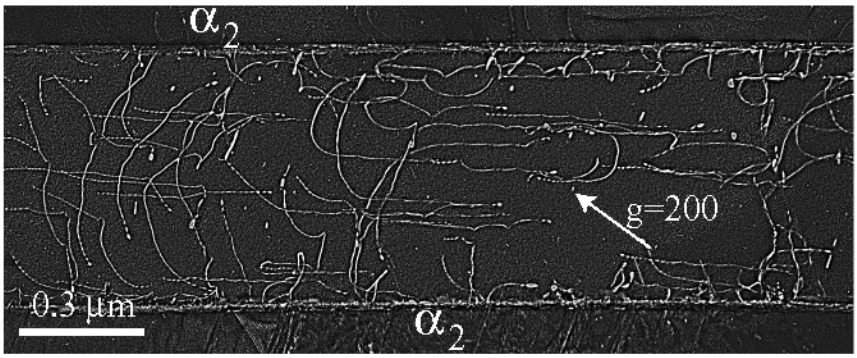

Figure 2

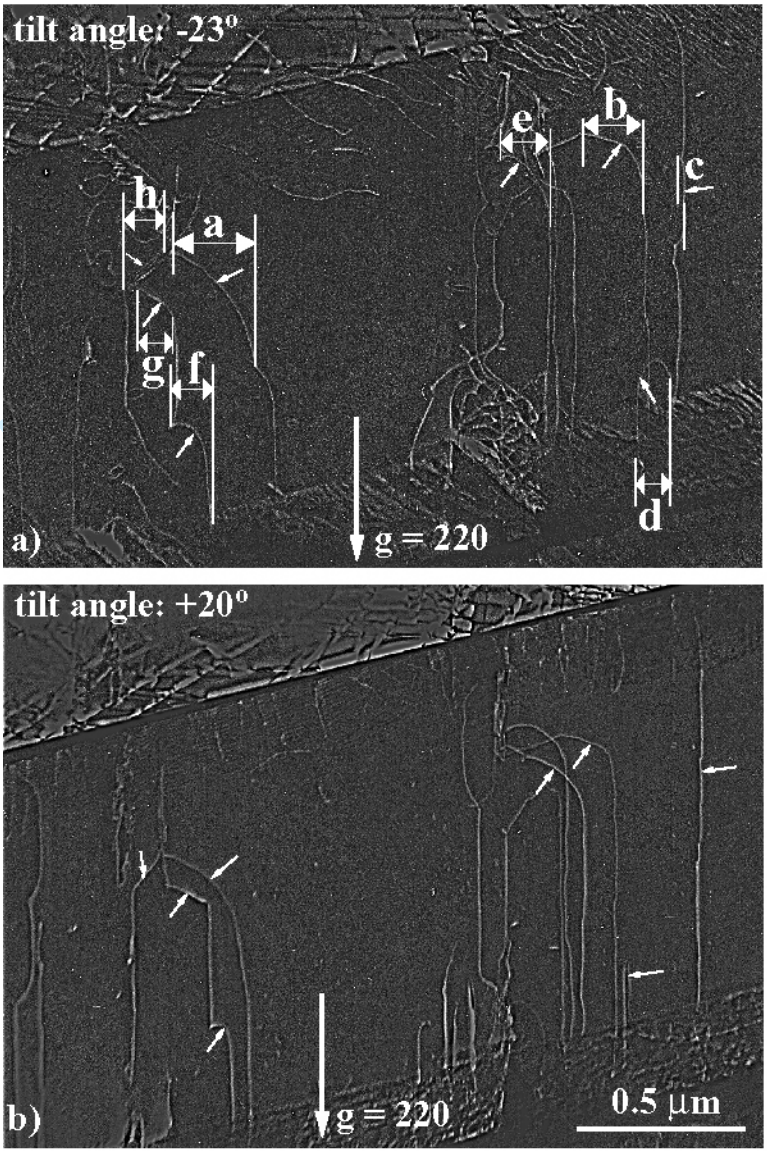

Figure 3

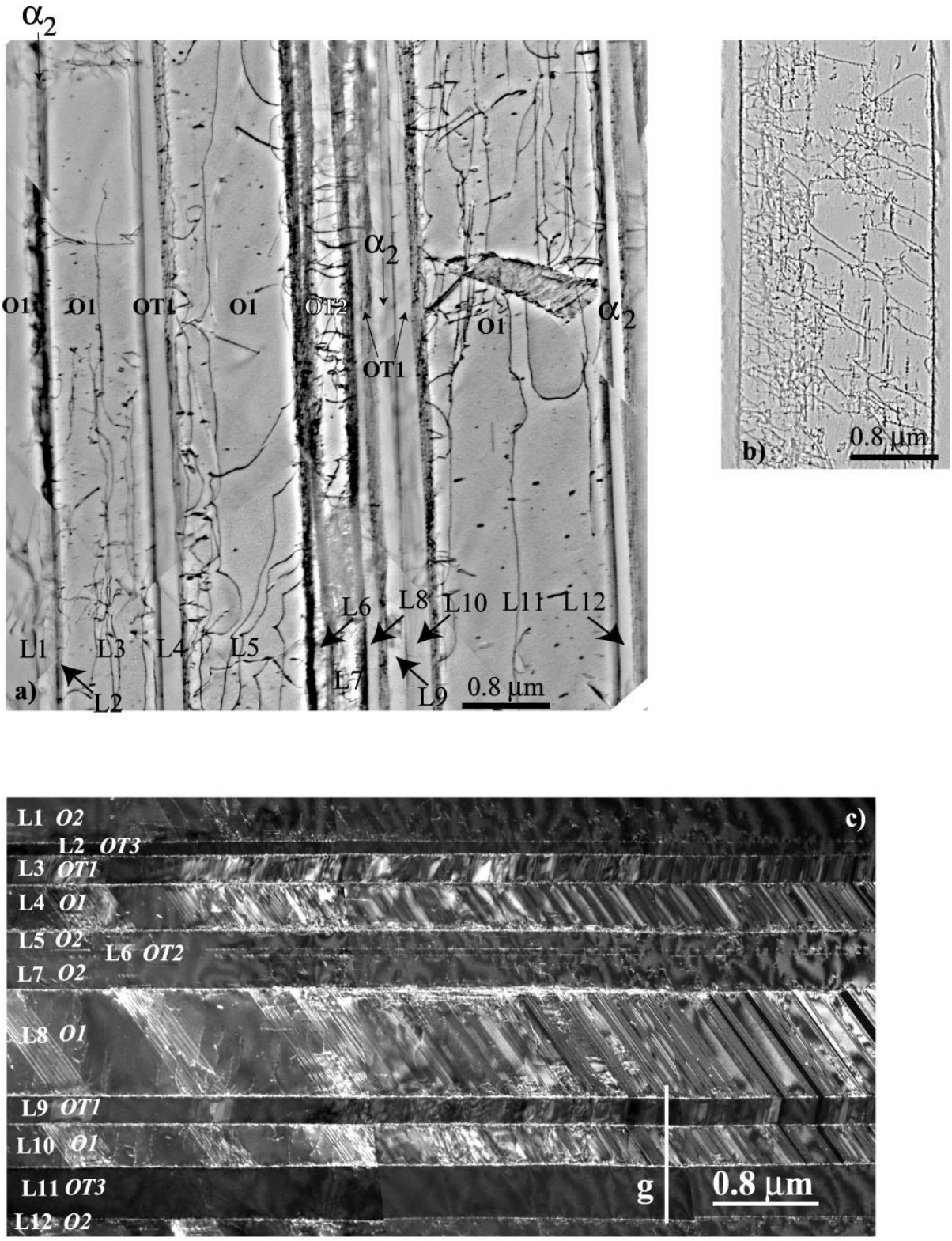
α2
O1
O1
OT1
O1
OT2
α2
O1
α2
OT1
L6
L8
L10
L11
L12
L1
L3
L4
L5
L7
L9
L2
a)
0.8 μm
b)
0.8 μm
c)
L1 O2
L2 OT3
L3 OT1
L4 O1
L5 O2
L6 OT2
L7 O2
L8 O1
L9 OT1
L10 O1
L11 OT3
L12 O2
g
0.8 μm

Figure 4

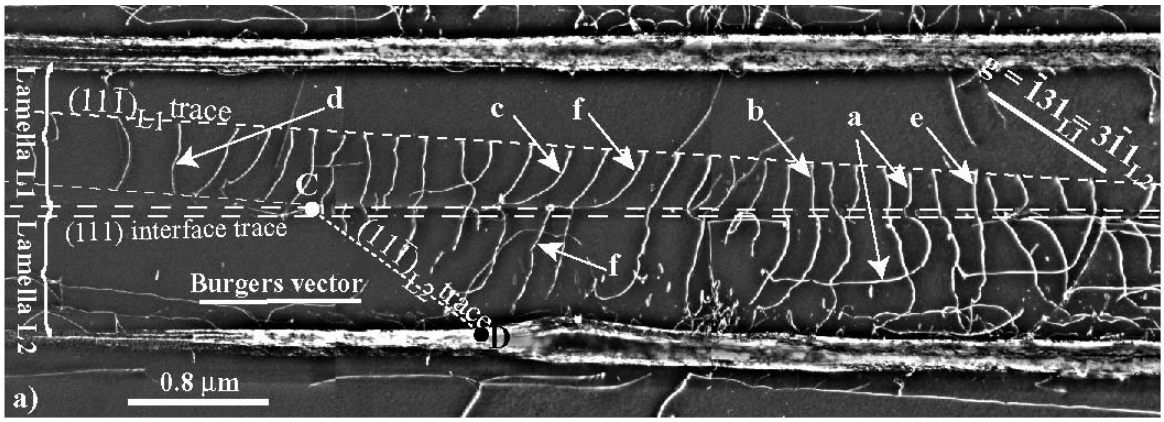
Lamella L1
Lamella L2
$(11\bar{1})_{L1}$ trace
d
c
f
b
a
e
$g = \bar{1}31_{1\bar{1}}\bar{3}\bar{1}1_{L2}$
C
(111) interface trace
$(11\bar{1})_{L2}$ trace
Burgers vector
f
D
0.8 μm
a)

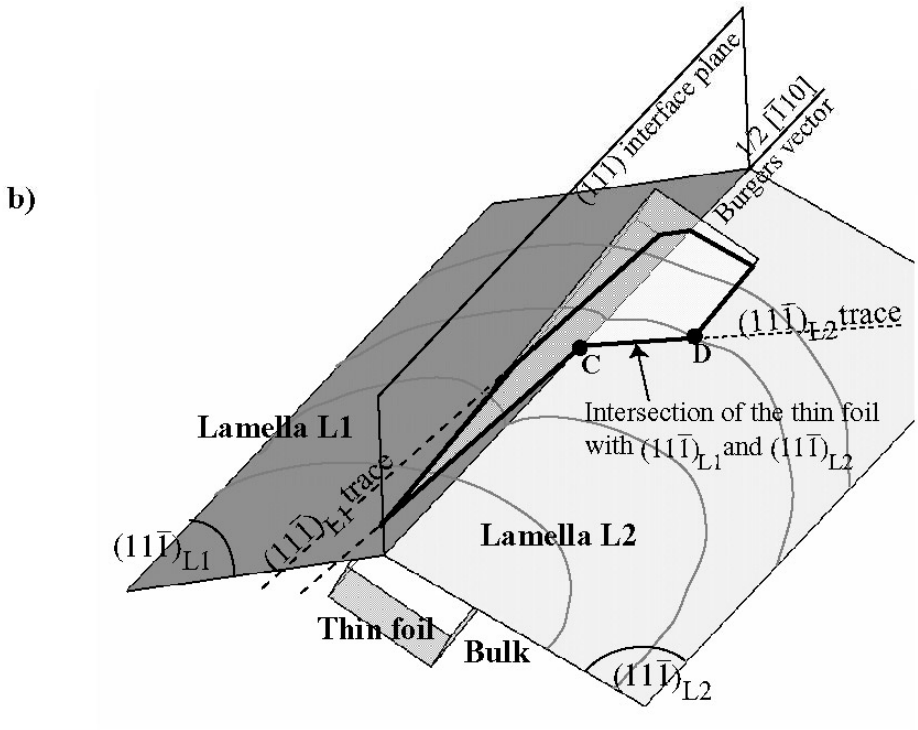
b)
(111) interface plane
1/2 [$\bar{1}$10]
Burgers vector
$(11\bar{1})_{L2}$ trace
C
D
Intersection of the thin foil
with $(11\bar{1})_{L1}$ and $(11\bar{1})_{L2}$
Lamella L1
$(11\bar{1})_{L1}$ trace
$(11\bar{1})_{L1}$
Lamella L2
Thin foil
Bulk
$(11\bar{1})_{L2}$

Figure 5

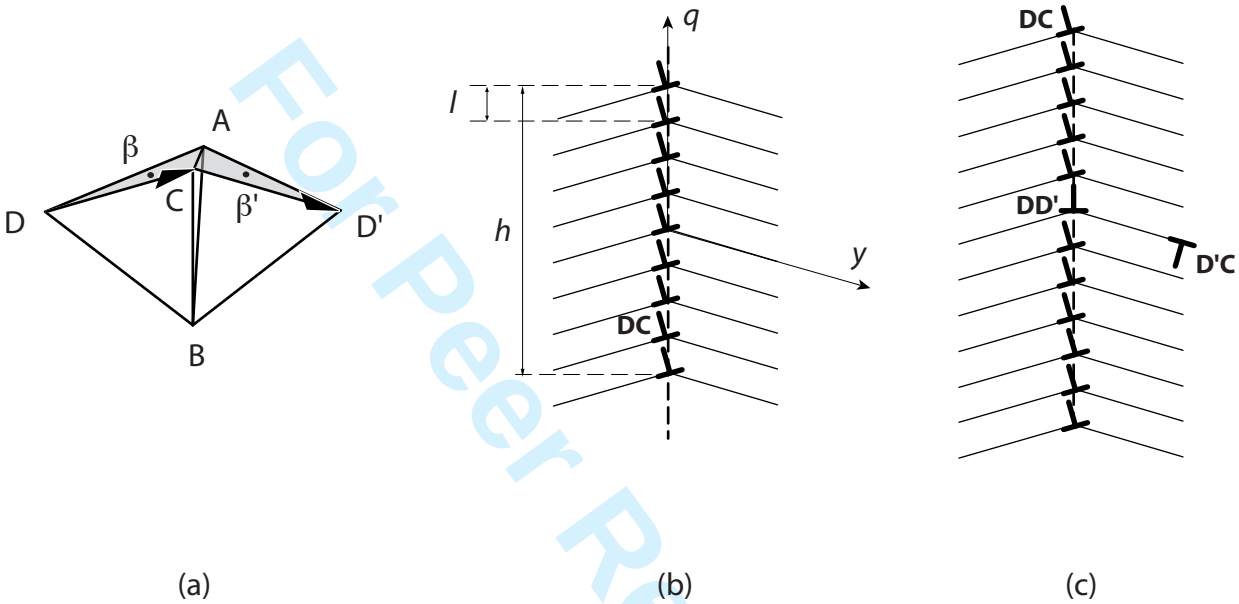

(a) (b) (c)

Figure 6

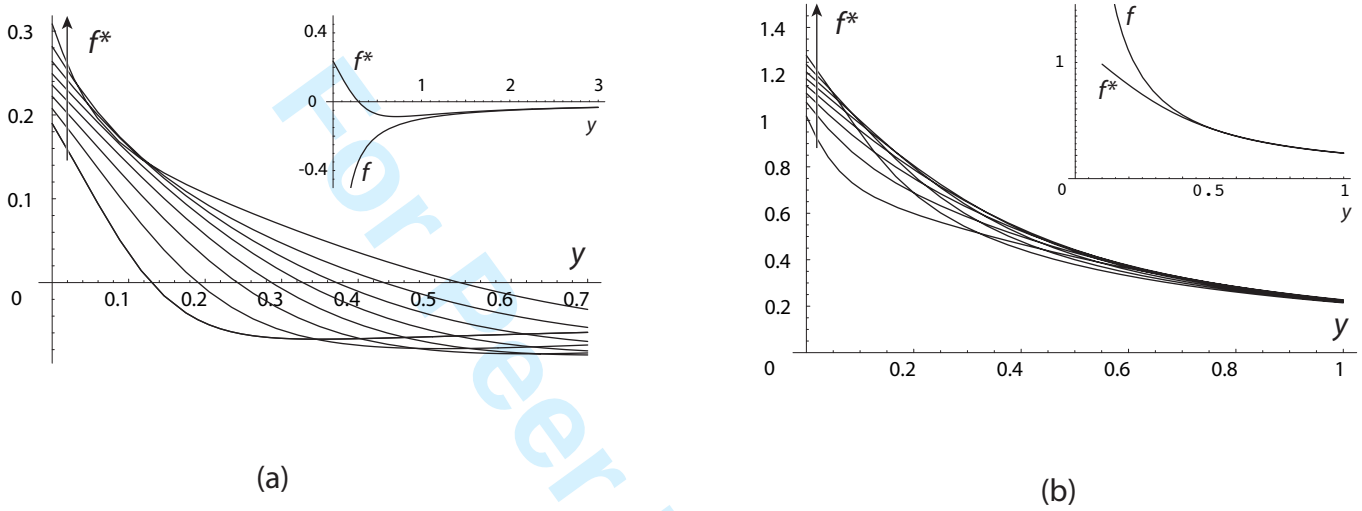

Figure 7